



Measuring molecular singlet oxygen (${}^1\text{O}_2^*$) from atmospheric photosensitzers: Intercomparison of techniques, irradiation setups, data analysis and protocol recommendations

Keighan J. Gemmell¹, Laura Marie Dahler Heinlein², Emma A. Petersen-Sonn³, Claudia Sardena¹, Zhongyu Guo³, Nory Mariño-Ocampo⁴, Belinda Heyne⁴, Christian George³, Cort Anastasio², and Nadine Borduas-Dedekind¹

¹Department of Chemistry, University of British Columbia, Vancouver, V6T 1Z1, Canada

²Department of Land, Air and Water Resources, University of California, Davis, CA 95616, USA

³Universite Claude Bernard Lyon 1, CNRS, IRCELYON, UMR 5256, Villeurbanne, F-69100, France

⁴Department of Chemistry, University of Calgary, 2500 University Drive NW, Calgary, AB T2N 1N4, Canada

Correspondence: Nadine Borduas-Dedekind (borduas@chem.ubc.ca)

Abstract. Molecular singlet oxygen (${}^1\text{O}_2^*$) is the first excited state of molecular oxygen (O_2) and can be formed through indirect photochemistry during irradiation of chromophoric organic matter. Once formed in the particle and droplet phases in the atmosphere, ${}^1\text{O}_2^*$ can be a competitive oxidant in the photochemical processing of organic matter. Yet, as more researchers study the atmospheric photochemistry of ${}^1\text{O}_2^*$, it is useful to establish protocols by evaluating and comparing experimental setups across laboratories. Here, we present ${}^1\text{O}_2^*$ measurements from 4 photosensitizing molecules in 4 photoreactor setups at 3 research institutions, including two xenon lamps of different strengths and two multi-bulb UVA + UVB broadband systems. The production of ${}^1\text{O}_2^*$ was investigated from perinaphthenone, lignin, and juglone, which are photosensitizers with atmospherically relevant light absorbing moieties, as well as from Rose Bengal, a standard photosensitizer. Two chemical actinometers, 2-nitrobenzaldehyde and p-nitroanisole/pyridine, were used to quantify photon fluxes and calculate rates of light absorbance for photosensitizers for each photoreactor. We compared two commonly used ${}^1\text{O}_2^*$ quantification methods, chemical probe method using furfuryl alcohol, as well as direct ${}^1\text{O}_2^*$ phosphorescence detection at 1270 nm. Rates of light absorbance across experimental setups for each photosensitizer ranged between 0.2 and 62×10^{-5} mol_{photons} L⁻¹ s⁻¹, while ${}^1\text{O}_2^*$ steady-state concentrations ranged between 0.01 and 129×10^{-11} M. Despite order of magnitude differences in rate of light absorbance and ${}^1\text{O}_2^*$ steady state concentrations, normalizing to ${}^1\text{O}_2^*$ quantum yields showed good inter-laboratory agreement but only for perinaphthenone ($94\% \pm 9\% - 112\% \pm 17\%$) and for Rose Bengal ($67\% \pm 15\% - 87\% \pm 5\%$). ${}^1\text{O}_2^*$ quantum yields for lignin and juglone increased with decreasing irradiation wavelength, consistent with a wavelength-dependence. Finally, we make five recommendations to improve the accuracy and reproducibility of ${}^1\text{O}_2^*$ measurements. These include considering wavelength-dependent quantum yields, avoiding suppression of ${}^1\text{O}_2^*$, controlling and reporting photoreactor temperature, considering light scattering from nanoparticles, and conducting control experiments. These recommendations will help standardize ${}^1\text{O}_2^*$ measurements in studying photochemical processing of atmospheric aerosols and droplets.



1 Introduction

Wildfires are becoming more frequent and severe with rising global temperatures, affecting air quality, climate, and human health (Tymstra et al., 2020). These events are major sources of brown carbon (BrC) aerosols, which contain light-absorbing organic chromophores capable of driving complex photochemistry in the atmosphere (Laskin et al., 2015). Upon absorbing 25 sunlight, these chromophores reach electronically excited states that can transfer energy to other atmospheric species, initiating indirect oxidation pathways (George et al., 2015; Li et al., 2022; Hems et al., 2021). One particularly important pathway is the formation of triplet excited state organic carbon ($^3\text{C}^*$) and its subsequent energy transfer to molecular oxygen, generating singlet oxygen ($^1\text{O}_2^*$), a potent but oxidant (Kaur and Anastasio, 2018; McNeill and Canonica, 2016). Excited-state oxidants have been hypothesized to contribute to the elevated oxidation state of carbon observed in wildfire plumes, beyond what can 30 be explained by classical radical chemistry (Akherati et al., 2022).

$^1\text{O}_2^*$ is efficiently generated by well-characterized synthetic photosensitizers such as Rose Bengal and Methylene Blue (Wilkinson et al., 1993), including within the context of photo-dynamic therapy (Gianotti et al., 2014; Dhaini et al., 2022). In natural waters, dissolved organic matter is a strong photosensitizer, with quinones, aldehydes, ketones, coumarins, and polycyclic aromatic hydrocarbons among the compound classes responsible for $^1\text{O}_2^*$ production (McNeill and Canonica, 2016). 35 Atmospheric BrC contains chemical analogues of these same chromophores, including nitrophenols (Xu et al., 2022), nitroanisoles (Zheng et al., 2023; Li et al., 2025b), quinones (Lee et al., 2014), and aromatic carbonyls (Smith et al., 2014, 2016), though their photosensitizing activity remains incompletely characterized. Measurements of $^1\text{O}_2^*$ across atmospheric samples such as fog water (Anastasio and McGregor, 2001; Kaur and Anastasio, 2017), cloud and rainwater (Faust and Allen, 1992; Albinet et al., 2010), indoor cooking aerosols (Borduas-Dedekind et al., 2024), road dust (Cote et al., 2018; Burnett et al., 40 2025), and particulate matter extracts (Manfrin et al., 2019; Ma et al., 2023b; Lyu et al., 2023; Bogler et al., 2022; Cote et al., 2018; Kaur et al., 2019a; Leresche et al., 2021) confirm that $^1\text{O}_2^*$ is ubiquitous in multiphase atmospheric environments. Recent studies also demonstrate $^1\text{O}_2^*$ reactivity at air–solid and air–water interfaces (Durantini et al., 2023; Durantini and Greer, 2021; Li et al., 2025a).

Concentrations of $^1\text{O}_2^*$ are typically on the order of 10^{-13} M (Bogler et al., 2022; Cole et al., 2018; Kaur et al., 2019b; 45 Leresche et al., 2021; Lyu et al., 2023; Ma et al., 2023b, a; Manfrin et al., 2019; Heinlein et al., 2025), an order of magnitude larger than its triplet excited state precursor (10^{-14} M) (Kaur et al., 2019b; Lyu et al., 2023; Ma et al., 2023b, a) and two orders of magnitude larger than $\cdot\text{OH}$ (10^{-15} M) (Arakaki et al., 2013; Kaur et al., 2019b; Leresche et al., 2021; Ma et al., 2023b, a; Zhou et al., 2008) in atmospheric extracts. Yet, reported $^1\text{O}_2^*$ quantum yields vary widely, even for the same material. For 50 example, Suwannee River fulvic acid shows quantum yields ranging from 0.47 to 5.4%, with strong wavelength dependence (Partanen et al., 2020). Atmospheric samples likewise span 0.2–19% (Ma et al., 2023a; Petersen-Sonn et al., 2025; Kaur et al., 2019b; Bogler et al., 2022; Manfrin et al., 2019; Ma et al., 2024; Lyu et al., 2023). Some of these discrepancies arise from using different rate constants, different parameters for light absorbance, dismissing the presence of competing oxidants, or measurement errors (Ossola et al., 2021).



The challenge of extrapolating laboratory measurements of $^1\text{O}_2^*$ to the atmospheric context is exacerbated by the current
55 lack of reproducibility, making it difficult to distinguish between variability in $^1\text{O}_2^*$ measurements and true inconsistencies in reproducibility. Anton et al. (2024) recently reported an intercomparison study in surface water context related to photochemical processes and made suggestions on how to limit the uncertainty related to the wavelength-dependence of quantum yields. Indeed, two extensive reviews have been written in the aquatic context to help reduce measurement reporting discrepancies by
56 Ossola et al. (2021); Anton et al. (2024). Our study builds on their work as we consider the atmospheric context of measuring excited state oxidants.

To evaluate atmospheric measurement consistency, we selected a diverse set of BrC-relevant photosensitizers: perinaphthenone, juglone, and lignin (Fig. 1). Perinaphthenone is a benchmark $^1\text{O}_2^*$ sensitizer with well defined photophysics (Schmidt et al., 1994; Schweitzer and Schmidt, 2003) and structurally similar to BrC moieties (Samburova et al., 2016). Juglone represents hydroxyquinones which have been proposed to be atmospheric photosensitizers linked to BrC formation (Lee et al., 2014; Manfrin et al., 2019). Lignin and its derived products are present in biomass burning organic aerosols, (Myers-Pigg et al., 2016; Shakya et al., 2011) and can generate $^1\text{O}_2^*$ upon irradiation (Du et al., 2018; Fleming et al., 2020). For a standard comparison, we also included Rose Bengal as a well studied reference sensitizer commonly used to benchmark $^1\text{O}_2^*$ quantum yields, albeit an atmospherically irrelevant molecule (Redmond and Gamlin, 1999; Gottschalk et al., 1986).

Here, we quantified $^1\text{O}_2^*$ production from four photosensitizers in four photoreactor setups across three institutions to establish a standard operating procedure for atmospheric chemistry experiments. To compliment our inter-laboratory photoreactor intercomparison, we also measured $^1\text{O}_2^*$ quantum yields using phosphorescence spectroscopy to act as a method comparison to chemical probe quantification. Standardizing a method of $^1\text{O}_2^*$ measurement is timely, as the there are increasing numbers of studies of photooxidants in irradiated particulate matter (Heinlein et al., 2025; Chang et al., 2025). This study is unique in its direct intercomparison of $^1\text{O}_2^*$ quantification using the identical photosensitizing molecules and procedures across different photoreactor setups. Following this intercomparison, we provide recommendations to standardize $^1\text{O}_2^*$ measurements to minimize errors and enhance interpretation of results specifically across different light sources. Our goal is to provide a methodological road map for future studies to consider and adopt in the measurements of photooxidants with a focus on $^1\text{O}_2^*$ in atmospherically relevant samples.

2 Methods

80 2.1 Chemicals

Isopropanol (HPLC grade, $\geq 99.9\%$), perinaphthenone (97%), juglone (5-hydroxy-1,4-naphthoquinone, 97%), lignin (low sulphonate alkali lignin), 4-nitrophenol (98%), 2-nitroanisole (98%), 3-nitroanisole (98%), 4-nitroanisole (98%), Rose Bengal (95%), 2-nitrobenzaldehyde (2NB, 98%), and pyridine (Pyr, $>99.9\%$) were all purchased from Sigma-Aldrich and used without further purification. All solutions were prepared using $18.2\text{ M}\Omega\text{-cm}$ Milli-Q water.

85 Furfuryl alcohol (FFA, 97%) and p-nitroanisole (PNA, 97%) were checked for purity using UV-Vis, and purified if coloured impurities were present. Specifically, FFA was purified using a liquid-liquid extraction with NaHCO_3 , followed by fractional



distillation under reduced pressure (see Fig. S20 for the impact of FFA impurities on control experiments) (Armarego and Chai, 2013). FFA was then stored in the fridge and covered in foil to avoid any photochemical processes. PNA was recrystallized from petroleum ether at 60 °C (Armarego and Chai, 2013).

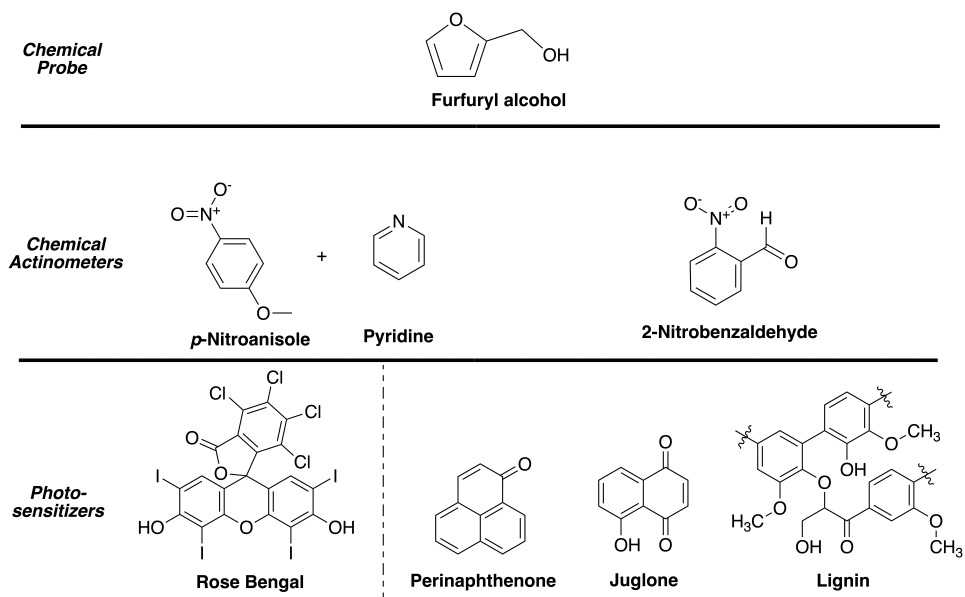


Figure 1. Structures of chemicals used in this study. Top row: chemical probe, furfuryl alcohol (FFA). Middle row: chemical actinometers, p-nitroanisole (PNA)/ pyridine (Pyr), and 2-nitrobenzaldehyde (2NB). Bottom row: photosensitizers. Rose Bengal is a synthetic dye standard and perinaphthenone, juglone, and lignin are atmospherically relevant moieties.

90 2.2 Instruments

In this section, we describe the details of each photoreactor at the University of British Columbia (UBC), University of California Davis (UCD), and Universite Claude Bernard Lyon 1 (Ircelyon), as well as high performance liquid chromatograph (HPLC), UV/Vis spectrometer and spectrophotometer at each institution.

2.2.1 Photoreactor experimental setups

95 **UBC** - The photoreactor used at UBC was a Rayonet RPR-200 (The Southern NE Ultraviolet Co.) equipped with 16 removable bulbs and a rotating sample carousel (Fig. 2a). The photoreactor was temperature controlled using the vented gas from a 15 L liquid nitrogen dewar (Cryofab, Inc. CLPB-15-GF). Temperature was monitored using a thermocouple probe (Thermosense BTM-4208SD 12 Channels Temperature Recorder) at each time-point. Experimental solutions (5 mL) were transferred into borosilicate glass test tubes and set into a rotating carousel. Empty slots on the carousel were filled with borosilicate glass 100 vials containing 5 mL of MilliQ water in order to ensure homogeneous light distribution. 20 μ M furfuryl alcohol, 1 mM of isopropanol and 10 μ M of either perinaphthenone, Rose Bengal, juglone, or 20 mg/L of lignin were used to make up



experimental solutions. At 6-10 designated time points during illumination, 100 μ L aliquots were removed for furfuryl alcohol quantification. Two UBC photoreactor setups were used for the present study. One setup used 12 UVA centred bulbs (Southern NE Ultraviolet Co., RPR-3500A), herein referred to as UBC UVA. The other setup used 8 UVA centred bulbs and 8 UVB centred bulbs (Zoo Med 26396 Reptisun 15 W 10.0 T5-Ho UVB Fluorescent Lamp, 12"), herein referred to as UBC UVA+UVB broadband.

105 UCD - At UCD, tropospheric sunlight was simulated with a 1000 W xenon arc lamp with three downstream optical filters: a water filter, an AM1.0 air mass filter (AM1D-3L, Sciencetech), and a 295 nm long-pass filter (20CGA-295, Thorlabs) (Fig. 2b). The temperature of the illumination chamber was controlled with a water bath set to 20 $^{\circ}$ C. Illuminations were either 110 performed in 1 mL GE 021 quartz tubes (5 mm inner diameter) or in 5 mL rectangular quartz cuvettes (1 cm pathlength; Starna Cells). 20 μ M furfuryl alcohol, 1 mM of isopropanol and 10 μ M of either perinaphthenone, Rose Bengal, juglone, or 20 mg/L of lignin were used to make up experimental solutions. At five designated time points during each illumination experiment, 130 μ L aliquots were removed for furfuryl alcohol quantification. For the experiments performed in 1 mL tubes, the entire solution was illuminated. The solutions did not need to be stirred during illumination but the solutions were shaken vigorously prior 115 to aliquot removal. For the experiments performed in cuvettes, the light beam only illuminated a subset of the solution and therefore the solutions were stirred during illumination. The volume removed during the cuvette experiments did not exceed 15% of the initial illuminated volume.

120 Ircelyon - The set-up applied in Ircelyon consisted of a glass photoreactor equipped with a water jacket to allow for temperature control (Fig. 2c). 20 μ M furfuryl alcohol, 1 mM of isopropanol and 10 μ M of either perinaphthenone, Rose Bengal, or 30 μ M juglone, or 40 mg/L of lignin were used to make up experimental solutions. 20 mL of experimental solution were transferred to the photoreactor for irradiation. All experiments were performed at 293 K (20 $^{\circ}$ C). The solution was stirred by a magnetic stirrer. A quartz lid was placed on top of the reactor to avoid exchange with the air surrounding the set-up. The light source applied was a xenon lamp (LOT LSE140/160.25C, 150 W), which had an infrared (IR) filter, a mirror bending the light 90 $^{\circ}$, followed by a Pyrex filter to avoid light with wavelengths below 280 nm.

125 2.2.2 HPLC

130 UBC - High performance liquid chromatography (HPLC, Agilent 1260, Agilent Technologies) equipped with a photodiode array detector was used to quantify the decay of the photooxidant probes. The analytical method was conducted with a reverse phase C18 column (Agilent, 5 μ m, 4.6 \times 150 mm) and an eluent gradient of acetonitrile (ACN) and MilliQ water for furfuryl alcohol. For the furfuryl alcohol quantification, a flow rate of 1 mL min $^{-1}$ was used. The gradient was 6 minutes at 20/80 (water/ACN), and 2 minutes at 90/10 (water/ACN) for a total run duration of 8 min. Furfuryl alcohol was monitored at 219 nm and typically observed at 3.32 minutes (Bogler et al., 2022). For the monitoring of 2-nitrobenzaldehyde, a flow rate of 0.5 mL min $^{-1}$ was applied to an isocratic gradient of 60/40 (water/ACN), and maintained for 20 minutes. 2-nitrobenzaldehyde was monitored at 254 nm and was typically observed at 9.6 minutes. For p-nitroanisole, the gradient was 6 min at 50/50 acetonitrile/acetate buffer (pH=6). The p-nitroanisole peak was typically quantified at 316 nm.

135 UCD - Furfuryl alcohol was monitored using high pressure liquid chromatography (HPLC: Shimadzu LC-20AB pump, Thermo



Scientific Accucore XL C18 column (50 × 3 mm, 4 μ m bead), and Shimadzu-M20A Photodiode Array detector. A flow rate of 0.45 mL min⁻¹ and an eluent gradient with 2 minutes of 10/90 (acetonitrile/water), 3.5 minutes of 40/60 (acetonitrile/water), and the remaining 12.5 minutes with 10/90 (acetonitrile/water) for a total run time of 18 minutes was used. Furfuryl alcohol was quantified at 210 nm and eluted at 3.0 minutes, and the remainder of the run was to ensure all photosensitizers were flushed

140 from the column.

Ircelyon - Samples were extracted at varying time intervals, depending on the experiment, and set aside for UHPLC/UV analysis. The method applied for UHPLC/UV analysis had an ACQUITY UPLC HSS T3 by WATERS column (100 mm × 2.1 mm, 1.8 μ m) and is also described in Petersen-Sonn et al. (2024). With a flow of 0.3 mL min⁻¹ the method started using two solvents: H₂O with 0.1% formic acid (solvent A), and acetonitrile (ACN) with 0.1 % formic acid (solvent B). Initially, 145 1% solvent B (and 99% solvent A) was applied for 2 min. In the next 11 min, the gradient gradually shifted from 1 to 100 % solvent B. After this, solvent B was kept at 100 % for the following 2 min, which was followed by a change to 1 % solvent B (over 0.1 min), which was kept until the end of the sequence (total runtime of 22 min). This allowed for an equilibrium of the column before the next sample was injected. Furfuryl alcohol, 2-nitrobenzaldehyde and p-nitroanisole were analyzed at 218, 254, and 320 nm, respectively.

150 2.2.3 UV/Vis spectroscopy

All absorbance spectra of experimental solutions was measured from 200 - 800 nm and contained furfuryl alcohol, isopropanol, the photosensitizer. Samples were measured in 1 cm pathlength quartz cuvettes, and were corrected for baseline and for the absorbance of a blank furfuryl alcohol + isopropanol solution to isolate the absorbance of the photosensitizer. At UBC, absorbance spectra were recorded using a double beam UV/Visible spectrometer (Carry 5000, Varian). At UCD, absorbance 155 spectrum of each sample solution were measured with a Shimadzu UV-2501PC spectrophotometer. At Ircelyon, solutions were measured using an Agilent Cary 60 spectrophotometer.

2.2.4 Photospectrometers

An Ocean Optics FLAME-T-UV-VIS spectrophotometer equipped with a QP600-1-XSR fiber optic cable and a CC-3-UV-S cosine receptor was used to measure the irradiance spectrum of the photoreactor setups at UBC. Due to the rotation of the 160 carousel sample holder, the spectrophotometer probe was positioned in one of the sample slots and rotated for measurement. One rotation of the sample carousel took 10 s. To not oversaturate the spectrophotometer detector and to obtain the entire photoreactor light output the spectrophotometer integration time was set to 0.25 s and averaged over 40 scans. At UCD, a TIDAS S 300 VIS/NIR 3011 (MMS 300-1100 nm) spectrophotometer was used to measure the irradiance spectrum of the solar simulator. The Ircelyon laboratory used an Avantes AVASPEC-HSC1024 x 58TEC-EVO spectrophotometer, equipped 165 with an optical fiber (FC-UV/IR-400-1-PR, Avantes) that has a cosine corrector, was employed to measure the irradiance spectrum of the lamp.



2.3 Quantifying $^1\text{O}_2^*$ formation parameters

2.3.1 Rate of light absorbance

The rate of light absorbance (R_{abs} , $\text{mol}_{\text{photons}} \text{cm}^{-2} \text{s}^{-1}$) of the photosensitizer was calculated by:

170 $R_{\text{abs}} = \sum_{\lambda} (I_{\lambda,0} \cdot \text{abs}_{\lambda} \cdot 2.303 \cdot 10^3)$ (1)

where abs_{λ} is absorbance of the sample (cm^{-1} , baseline corrected), $I_{\lambda,0}$ is the spectral irradiance of the light source ($\text{mol}_{\text{photons}} \text{cm}^{-2} \text{s}^{-1} \text{nm}^{-1}$), and the values 2.303 and 10^3 are conversions for base and units, respectively (Kaur et al., 2019b). Following the recommendations of Ossola et al. (2021), UV-vis spectra were corrected by averaging and subtracting the absorbance of a sample from 700-800 nm (or the region of noise determined in logarithmic absorbance space of the UV-Vis spectrum) from the 175 entire absorbance spectra. Additionally, negative absorbance values were screened and set to be 0 to avoid an artificial decrease in the rate of light absorbance. A baseline spectrum was also taken with the solvent (water) as well as isopropanol and furfuryl alcohol.

2.3.2 $^1\text{O}_2^*$ production under pseudo-first-order conditions

$^1\text{O}_2^*$ was detected using furfuryl alcohol as a chemical probe, which has a well constrained rate constant with $^1\text{O}_2^*$ of $1 \times 10^8 + 180 2.1 \times 10^6 (T[^\circ\text{C}] - 22) \text{ M}^{-1} \text{ s}^{-1}$ (Appiani et al., 2017) and has been used for several decades for $^1\text{O}_2^*$ quantification (Haag et al., 1984). The decay of the furfuryl alcohol probe was followed with (U)HPLC/UV. The loss of the $^1\text{O}_2^*$ probe, furfuryl alcohol, can be expressed as:

$$-\frac{d[\text{FFA}]}{dt} = k_{\text{FFA} + ^1\text{O}_2^*} \times [\text{FFA}] \times [^1\text{O}_2^*]_{\text{ss}} + k_{\text{FFA} + ^3\text{C}^*} \times [\text{FFA}] \times [^3\text{C}^*]_{\text{ss}} + k_{\text{FFA} + \cdot\text{OH}} \times [\text{FFA}] \times [\cdot\text{OH}]_{\text{ss}} + j_{\text{FFA}} \quad (2)$$

The reaction of furfuryl alcohol with hydroxyl radicals ($\cdot\text{OH}$) was set to be 0 due to the use of a quencher (Bogler et al., 185 2022), and the direct photodegradation (j_{FFA}) was also negligible for the irradiance times used in this study, evidenced by the direct photodegradation control experiments (Fig. S1). The reaction of furfuryl alcohol with $^3\text{C}^*$ is also negligible, evidenced by deoxygenation control experiments (Fig. S2). Therefore, the loss of furfuryl alcohol can then be expressed only as a function of its reaction with $^1\text{O}_2^*$.

$$\ln \left(\frac{[\text{FFA}]_t}{[\text{FFA}]_0} \right) = k_{\text{FFA} + ^1\text{O}_2^*} \times [^1\text{O}_2^*]_{\text{ss}} \times t = k_{\text{obs,FFA}} \quad (3)$$

190 Through this decay, the pseudo-first-order rate constant, $k_{\text{obs,FFA}}$, was obtained (Fig. S2-S7). $k_{\text{obs,FFA}}$ was then corrected for light screening of the sample:

$$k_{\text{obs,corr}} = \frac{k_{\text{obs,FFA}}}{\text{sf}} \quad (4)$$



2.3.3 Light screening factor

The light screening of the sample depends on the light absorbance of the sample, the path length of the light through the sample,

195 and the irradiance from the light source. The light screening factor (sf) is described by Eq. 5.

$$sf = \frac{\sum((1 - 10^{-abs_{\lambda} \cdot l}) I_{\lambda,0})}{\sum(2.3 \cdot abs_{\lambda} \cdot l \cdot I_{\lambda,0})} \quad (5)$$

where l is the path length of the sample. As described in Equation 4, the screening factor was used to obtain the corrected rate constant for decay of furfuryl alcohol, $k_{obs,corr}$. $k_{obs,corr}$ was used to calculate the steady-state $^1O_2^*$ concentration by applying the second-order rate constant between furfuryl alcohol and $^1O_2^*$, $k_{^1O_2^*,FFA}$, according to Equation 6.

$$200 \quad [^1O_2^*]_{ss} = \frac{k_{obs,corr}}{k_{^1O_2^*,FFA}} \quad (6)$$

2.3.4 $^1O_2^*$ quantum yield ($\Phi_{^1O_2^*}$)

The quantum yield expresses the efficiency of $^1O_2^*$ production, i.e., it is the fraction of absorbed photons that lead to $^1O_2^*$ production (Eq. 7).

$$\Phi_{^1O_2^*} = \frac{\# \text{ of } ^1O_2^* \text{ molecules formed}}{\# \text{ of photons absorbed}} \quad (7)$$

205 The quantum yield is particularly powerful for comparing $^1O_2^*$ production across different experimental setups (Ossola et al., 2021). For example, strong irradiation sources would produce larger absolute quantities of $^1O_2^*$ that are difficult to directly compare to weaker irradiation sources.

Considering the photophysical and chemical processes in the system, the $^1O_2^*$ quantum yield can be expressed in Eq. 8 (Sharpless, 2012; Schweitzer and Schmidt, 2003; Ossola et al., 2021):

$$210 \quad \Phi_{^1O_2^*} = \Phi_{ISC} \frac{k_{O_2}[O_2]}{k_d^T + k_{O_2}[O_2]} f_{\Delta} \quad (8)$$

where Φ_{ISC} is the fraction of excited singlet photosensitizer molecules that undergo intersystem crossing to the excited triplet state, $\frac{k_{O_2}[O_2]}{k_d^T + k_{O_2}[O_2]}$ is the fraction of $^3C^*$ that is quenched by O_2 , and f_{Δ} is the fraction of the quenching that leads to the formation of $^1O_2^*$.

In practice, two methods can be used to calculate $\Phi_{^1O_2^*}$. The direct method ($\Phi_{^1O_2^*}^{dir}$) uses rate of light absorbance as well as a rate constant to account for the deactivation of $^1O_2^*$ in the solvent (Eq. 9).

$$\Phi_{^1O_2^*}^{dir} = \frac{k_{obs,corr} \cdot k_d}{k_{^1O_2^*,FFA} \cdot R_{abs}} \quad (9)$$



where k_d is the deactivation of $^1\text{O}_2^*$ by water, $2.76 \times 10^5 \text{ s}^{-1}$ (Appiani et al., 2017). The direct quantum yield depends on the rate of light absorbance, R_{abs} , which were determined using spectral irradiances determined using actinometry of either 2-nitrobenzaldehyde or p-nitroanisole/pyridine.

220

In contrast, the relative quantum yield of $^1\text{O}_2^*$ ($\Phi_{^1\text{O}_2^*}^r$) does not require photon flux to be quantitatively measured, and only normalizes rate of light absorbance of a compound of interest to a reference compound. In this study, perinaphthenone (PN) was applied as reference compound. Perinaphthenone as a reference photosensitizer allows the normalization of the production of photooxidants and of the rate of absorbance for each experiment, due to possible slight changes in irradiation and/or 225 experimental setup, since it has a well characterized $^1\text{O}_2^*$ quantum yield (Schmidt et al., 1994). Additionally, the triplet state of perinaphthenone does not react with furfuryl alcohol which greatly simplifies steady-state and quantum yield calculations (Schmidt et al., 1994; Ossola et al., 2021).

$$\Phi_{^1\text{O}_2^*}^r = \frac{k_{\text{obs,corr}}}{k_{\text{obs,PN,corr}}} \frac{R_{\text{abs,PN}}}{R_{\text{abs}}} \Phi_{\text{PN}} \quad (10)$$

In Equation 10, $k_{\text{obs,PN,corr}}$ is the observed decay of furfuryl alcohol due to $^1\text{O}_2^*$ produced by perinaphthenone that has been 230 corrected for light screening, and $R_{\text{abs,PN}}$ is the rate of light absorbance from the perinaphthenone sample.

2.4 Control experiments

2.4.1 Blank control

Control experiments were performed to isolate the reaction of furfuryl alcohol + $^1\text{O}_2^*$ and eliminate any other sources of furfuryl alcohol degradation. A blank control containing MilliQ water and 20 μM of furfuryl alcohol was irradiated to ensure 235 the absence of probe decay due to impurities in the solvent (MilliQ water) or direct photodegradation of the chemical probe due to impurities. Based on the results of this control experiment, j_{FFA} in equation 2 was set to zero.

2.4.2 Dark control

A dark control solution was prepared for each set of photosensitizer experiments by adding a glass vial of sample solution covered with aluminum foil to protect the solution from irradiation. The dark control sample was conducted to account for any 240 potential reactions between the photosensitizer and the probe in the absence of light.

2.4.3 Deoxygenated control (N_2 purge)

In order to investigate potential reactions of the triplet state of the photosensitizer with furfuryl alcohol, deoxygenation experiments were conducted. The borosilicate tube was sealed with a septum and bubbled with N_2 for 15 min to evacuate O_2 dissolved in solution and present in the headspace. Throughout the irradiation process, the time points were taken by adding 245 a N_2 flow through the system, to maintain an inert environment. O_2 deoxygenation experiments were only conducted at the



UBC laboratory. Since the same photosensitizer compounds were used, any triplet state reactivity with furfuryl alcohol observed, or lack thereof, is expected to be reproducible across all laboratories. Based on the results of the deoxygenation control experiments, we set the value of $k_{\text{FFA}+^3\text{C}^*}$ to zero in equation 2.

2.5 $^1\text{O}_2^*$ phosphorescence detection

250 To complement chemical probe quantification of $^1\text{O}_2^*$, we also used phosphorescence spectroscopy to directly detect the emission of $^1\text{O}_2^*$. Since $^1\text{O}_2^*$ is in a spin-forbidden state, its relaxation to the ground state can be detected as phosphorescence emission. Corresponding to an energy gap of 94 kJ mol⁻¹ between the excited and ground states, this emission occurs in the near-infrared at a characteristic wavelength of 1270 nm. This distinct emission can be selectively filtered and monitored (Fig. S8). The instrumentation set up at the University of Calgary was a CryLas FTSS-355-Q3 Laser (532 nm and 355 nm 255 emission options, 1000 Hz pulse rate), Spectral Products CM110 Monochromator (set to 1270 nm detection), and a Hamamatsu H10330A-45 photomultiplier tube (Fig. S8). A bi-exponential fit of the data is used to obtain information about the generation of $^1\text{O}_2^*$, and the preceding triplet excited state of the photosensitizer (Kabanov et al., 2019).

$$S(t) = S_0 \frac{\tau_\Delta}{\tau_\Delta - \tau_T} \left(e^{\left(\frac{-t}{\tau_\Delta} \right)} - e^{\left(\frac{-t}{\tau_T} \right)} \right) + Y_0 \quad (11)$$

260 Where $S(t)$ is the signal intensity at time t , S_0 is signal intensity at time 0, τ_Δ is the $^1\text{O}_2^*$ lifetime, τ_T is the photosensitizer triplet lifetime, and Y_0 is the baseline correction. In order to determine a quantum yield of $^1\text{O}_2^*$ for different photosensitizers, and using an excitation wavelength of 355 nm, we measured signal intensity as a function of absorbance for a reference photosensitizer (in this case perinaphthenone) and compared each photosensitizer to the reference. The response of intensity as a function of absorbance was determined for the reference photosensitizer, then the quantum yield of the other photosensitizers can be determined by the same method (Equation 12).

$$265 \quad \Phi_{^1\text{O}_2^*, \text{sample}} = \frac{\text{slope}_{\text{sample}}}{\text{slope}_{\text{PN}}} * \Phi_{^1\text{O}_2^*, \text{PN}} \quad (12)$$

where slope is obtained as the linear regression of intensity response as a function of absorbance at the excitation wavelength. The standard error of the slope of the regression is reported as the uncertainty (Fig. S9). Phosphorescence measurements were conducted for five concentrations of each photosensitizing molecule dissolved in D₂O corresponding to absorbances of 0.1 to 0.5 AU. In addition to the photosensitizing molecules used for the photoreactor intercomparison study (Rose Bengal, 270 perinaphthenone, lignin, and juglone), a suite of nitroaromatic molecules (2-nitroanisole, 3-nitroanisole, 4-nitroanisole, and 4-nitrophenol) were also tested.

2.6 Chemical actinometers

Two chemical actinometers, 2-nitrobenzaldehyde and *p*-nitroanisole/pyridine, were used to determine the absolute photon flux in the sample container in each setup. The decay of the chemical actinometer as a function of irradiation time was followed



275 by (U)HPLC/UV detection to obtain the first-order rate constant, k_{obs} . The measured irradiance spectrum of the light source, $I_{\lambda,\text{meas}}$, was used to calculate a relative irradiance spectrum, $I_{\lambda,\text{rel}}$, according to Equation 13.

$$I_{\lambda,\text{rel}} = \frac{I_{\lambda,\text{meas}}}{\sum I_{\lambda,\text{meas}}} \quad (13)$$

With the relative irradiance spectrum, a scaling factor, γ , was calculated as described by Ossola et al. (2021) (Eq. 14):

$$280 \quad \gamma = \frac{k_{\text{obs}}[\text{comp}]_0 l}{\Phi_{\text{comp}} \sum I_{\lambda,\text{rel}} (1 - 10^{-\varepsilon_{\lambda}[\text{comp}]_0 l}) \Delta \lambda} \quad (14)$$

where $[\text{comp}]_0$ was the concentration of the compound at the start of the irradiation, l is the path length of the light, Φ_{comp} is the quantum yield of the compound, ε_{λ} is the extinction coefficient of the compound, and $\Delta \lambda$ is the wavelength increment (typically 1 nm). For *p*-nitroanisole the quantum yield was calculated by: $\Phi_{\text{PNA}} = 0.29[\text{Pyr}] + 2.9 \cdot 10^{-4}$ (Laszakovits et al., 2017), where [Pyr] is the concentration of pyridine used. For 2-nitrobenzaldehyde, $\Phi_{\text{2NB}} = 0.41 \pm 0.02$ (Galbavy et al., 2010).

285 Both chemical actinometer quantum yields are reported to be independent of wavelength.

The scaling factor was used to scale the relative irradiance to obtain absolute irradiance ($I_{\lambda,0}$) (Ossola et al., 2021), as shown in Equation 15.

$$I_{\lambda,0} = I_{\lambda,\text{rel}} \cdot \gamma \quad (15)$$

Absolute irradiance was then used to calculate a rate of light absorbance for each of the photosensitizing molecules for each 290 photoreactor. Absolute irradiance was also used to compare photoreactor light output to simulated sunlight conditions.

2.7 Comparison to atmospheric sunlight

The NCAR Tropospheric Ultraviolet and Visible (TUV) Radiation Model was used to simulate sunlight at solar noon for the summer solstice of 2025 in Vancouver (49.2827° N, 123.1207° W), Canada (June 20th, 13:14 local time) (https://www.acom.ucar.edu/Models/TUV/Interactive_TUV/). The measurement altitude was 5 km to represent the mid-troposphere, and 295 total irradiation was considered. Surface albedo was set to 0.1, overhead ozone column concentration was set to 300 du, cloud optical depth was set to 0, and aerosol optical depth was set to 0.235. Conversion factors to equivalent hours of sunlight for atmospherically relevant photosensitizers were calculated according to equation 16.

$$\text{Conversion Factor} = \frac{R_{\text{abs}}}{R_{\text{abs,sunlight}}} \quad (16)$$

2.8 Wavelength dependent quantum yield experiments

300 To test the wavelength dependence of $^1\text{O}_2^*$ quantum yields of lignin and juglone, wavelength dependent experiments were performed at UCD. The illumination experiments were performed with a 1000 W mercury-xenon arc lamp with a downstream



monochromator (Spectral Energy) and a 310 nm long-pass filter. The illumination chamber was temperature controlled with a water bath set to 25 °C. Samples were illuminated with 313, 334, and 366 nm light. Experiments were performed in 1 cm 305 Spectrocil quartz cells (Starna Cells, 1-Q-10-GL14-C) with a plastic cap. The cuvettes initially held 3 mL of sample, and at each illumination time point, 90 μ L of solution was removed to perform HPLC-PDA analysis of FFA. At each wavelength, we determined the $^1\text{O}_2^*$ quantum yield of lignin and juglone by illuminating solutions of 20 mg L⁻¹ lignin and 20 μ M FFA, and 20 μ M juglone and 20 μ M FFA, respectively. At each wavelength, actinometry was quantified by illuminating 10 μ M 2NB. The $^1\text{O}_2^*$ quantum yields were calculated using the direct method with 2NB actinometry following equation 9.

3 Results

310 3.1 Intercomparison of photoreactor experimental set ups

3.1.1 Light types

Intercomparing photoreactor light sources is essential for evaluating the reproducibility and atmospheric relevance of $^1\text{O}_2^*$ measurements across different laboratory setups, because light absorption by chromophoric organic matter is the first step in the formation of $^1\text{O}_2^*$. We compared xenon lamps as solar simulator systems at UCD (Heinlein et al., 2025) and at Irce-315 lyon (Petersen-Sonn et al., 2025), as well as two configurations 16 bulbs of broad-band UV lights in a commercial Rayonet photoreactor at UBC (Borduas-Dedekind et al., 2024) (Fig. 2, Table 1).

These choice of light source has advantages and disadvantages to consider. Xenon lamps produce a broad spectrum most similar to the solar spectrum, including the photochemically active UV range (280–400 nm). Xenon lamp photoreactors provide a better mimic of natural sunlight, but may be less suited for mechanistic, wavelength-specific experiments. In contrast, UV-320 centred bulbs enable selective irradiation in higher-energy UV regions, but fail to replicate the full spectral profile of solar irradiance (Sec. 3.2, Fig. 3b).

Although this intercomparison focuses on these four systems, many other photoreactors are also used in the community. Examples reported in recent atmospheric photochemistry studies include multiple 300 W xenon lamps (Mabato et al., 2022; Go et al., 2024; Liu et al., 2025), custom LED reactors equipped with discrete monochromatic LEDs (Wu et al., 2021), and 325 additional photoreactors with different power xenon-lamp sources. In Section 3.2.4, we quantify each photoreactors light source compared to natural sunlight, and in Section 3.3.8 we assess the potential wavelength dependence of $^1\text{O}_2^*$ formation. Together, these comparisons provide the foundation for interpreting inter-laboratory differences in $^1\text{O}_2^*$ production, while recognizing the broader diversity of photoreactor setups used across the community.

3.1.2 Number of samples per experiment

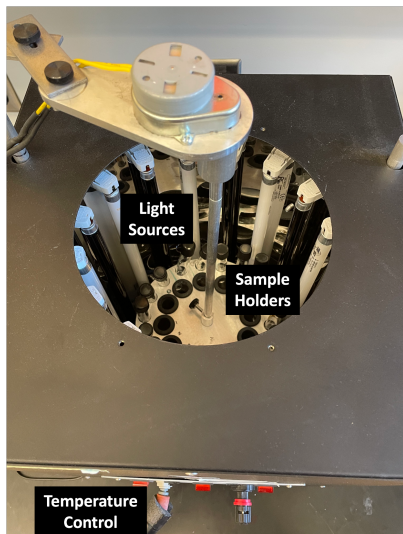
330 The number of samples that can be irradiated simultaneously depends on the light setup (Fig. 2, Table 1, column 4). If the setup has one point source, such as a xenon lamp, then only one sample can be irradiated at at time (Fig. 2b,c & S6). On the other hand, if the setup has multiple bulbs arranged in an array, like a Rayonet or an incubator, then dozens of samples can be



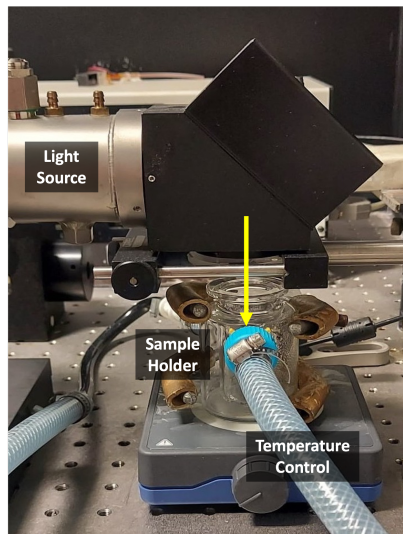
irradiated simultaneously. These multi-bulb setups can have a carousel, like the setup at UBC (Fig. S4), or have rotating lights (Fig. 2a). Multiple lights provide the advantage of increasing the experimental throughput. Additionally, chemical actinometry methods that were exposed to the exact same irradiation conditions were expected to provide the most accurate photon flux measurements, which is only possible when multiple samples can be irradiated simultaneously.
335

3.1.3 Temperature control

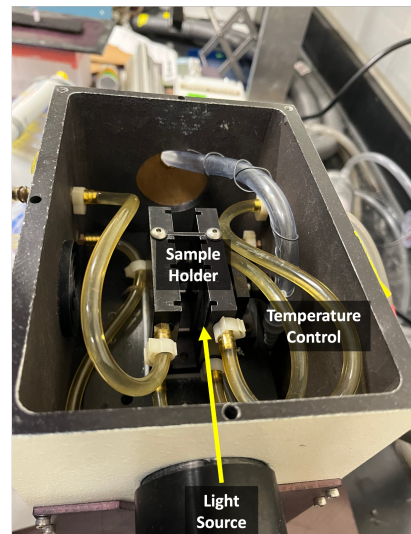
All three photoreactors can control sample temperature, which is important for chemical kinetic experiments, including for the reaction of $^1\text{O}_2^*$ with the common probe furfuryl alcohol. Indeed, Appiani et al. (2017) calculates a +2% increase in rate
340 constant per $^{\circ}\text{C}$ increase in temperature. The Rayonet temperature at UBC is measured using a thermal couple probe and is regulated using a perforated copper coil inside the photoreactor where liquid nitrogen flows through a needle valve (Fig. S4). However, this setup does not benefit from the same accuracy or temperature range that the water-cooled temperature regulators provide in the Ircelyon and UCD photoreactors (20-34 $^{\circ}\text{C}$ for the liquid nitrogen cooling system vs 0-50 $^{\circ}\text{C}$ for water bath cooling systems, Table 1). Operational temperatures used for intercomparison experiments in this work were 22 $^{\circ}\text{C}$ at UBC
345 and 20 $^{\circ}\text{C}$ at Ircelyon and UCD (Table 1, column 3).



(a) UBC



(b) Ircelyon



(c) UCD

Figure 2. Experimental setup of 3 different laboratory photoreactors. Showing panel a) UBC, b) Ircelyon, and c) UCD. Details of each photoreactor setup are shown in table 1. Main components of each set up, light source, sample holders, and temperature control, are labelled. Direction of light beam travel is indicated with a yellow arrow in panels b and c, and is in all directions in panel a.



Table 1. Photoreactor details for each laboratory. Light sources, temperature ranges, operational temperature used for this study, # of samples that can be irradiated simultaneously, and sample volumes.

Lab	Light Source	Temperature Control Range (°C)	Operational Temperature (°C)	# of Samples	Sample Volume (mL)
UBC	UVA, UVB, & Fluorescent	20-34	22	16	5
UCD	Xenon	0-50	20	1	1-20
Ircelyon	Xenon	0-50	20	1	20

3.2 Measuring irradiance

3.2.1 Comparing chemical actinometers

Chemical actinometry allows for the quantification of the photon flux from an irradiation source, necessary to intercompare photochemical results across samples, setups and studies. Chemical actinometers are compounds with well characterized direct 350 photolysis chemistry and with known quantum yields and absorption cross sections. For our intercomparison, we used two chemical actinometers: 2-nitrobenzaldehyde (Galbavy et al., 2010) and p-nitroanisole/pyridine (Laszakovits et al., 2017). Molar absorption coefficients for both compounds define the wavelength ranges over which they can be used as chemical actinometers, i.e., their validity ranges (Fig. S10). The validity ranges for the p-nitroanisole/pyridine system and for 2-nitrobenzaldehyde are 300–400 nm (Laszakovits et al., 2017), and 280–400 nm (Galbavy et al., 2010), respectively. For these actinometers to be 355 effective, these ranges should overlap with the emission spectra of the photoreactor, which is the case for our intercomparison (Sec. 3.1).

The p-nitroanisole (PNA) and pyridine (Pyr) actinometry pair has the advantage that the time decay can be adjusted from mins to h (depending on the strength of the light source) by varying the pyridine concentration (i.e. $\Phi_{\text{PNA}} = 0.29[\text{Pyr}] + 2.9 \cdot 10^{-4}$). For example, if the sample's furfuryl alcohol decay takes 12 h, the concentration of Pyr can be tuned to match 360 the timeline of the probe kinetics. In contrast, the quantum yield of the 2-nitrobenzaldehyde system is fixed ($\Phi_{\text{2NB}} = 0.41 \pm 0.02$) and cannot be tuned to match the timescale of ${}^1\text{O}_2^*$ probe decay experiments. For these reasons, when an experiment may be subject to varying photon flux over the irradiation period (for example, in natural sunlight experiments when the angle of the sunlight changes throughout the day), the p-nitroanisole/pyridine actinometer is preferred due to its tunable quantum yield. However, in the context of lab-based photoreactors, we found that 2-nitrobenzaldehyde was operationally simpler to use. If 365 photon flux is expected to remain stable throughout a ${}^1\text{O}_2^*$ probe experiment, the 2-nitrobenzaldehyde actinometer may be the more suitable option.

To demonstrate that these two chemical actinometers work interchangeably, we compared them across setups. As expected, they provided nearly identical photon fluxes as a function of wavelength for the same photoreactor (Fig. S11). Consequently, the rate of light absorbance of each photosensitizer in different photoreactor configurations did not differ by more than 11% 370 when using both chemical actinometers (Table S5). Nevertheless, we recommend conducting illumination experiments with



both 2-nitrobenzaldehyde (Galbavy et al., 2010) and p-nitroanisole/pyridine (Laszakovits et al., 2017) chemical actinometers at the start of a study, since the reproducibility of the photon fluxes determined by two independent actinometers provides confidence that the photon flux is accurately calculated. When the agreement is established, subsequent experiments may rely on a single actinometer.

375 **3.2.2 Photoreactor photon flux**

To compare the absolute and normalized photon fluxes from each setup, we measured their spectrally resolved irradiance profiles using a spectrophotometer. Absolute irradiance measurements were made using 2-nitrobenzaldehyde following equations 13–15. As a standard reference, we integrated the photon flux over 200–800 nm, noting that wavelengths below 290 nm contribute negligibly to tropospheric irradiance whereas wavelengths above approximately 600 nm are unlikely to initiate 380 photochemistry. The UCD photoreactor xenon light source had the highest absolute photon flux, with an integrated irradiance in the 200–800 nm wavelength range of 4686 W m^{-2} . (Fig. 3a). Significant internal reflections within the UCD photoreactor illumination chamber were also identified during this intercomparison and accounted for by using the 548 nm/347 nm intensity ratio (see details in the SI Sec. S11, Fig. S21). The Ircelyon photoreactor also used a xenon lamp, but produced a lower integrated irradiance at 171 W m^{-2} , consistent with the difference in xenon lamp power output of 150 W at Ircelyon compared 385 to 1000 W at UCD. The UBC photoreactor setups yielded a lower integrated irradiance of 103 W m^{-2} for the UVA configuration, and 163 W m^{-2} for the UVA+UVB broadband configuration. The tropospheric ultraviolet and visible (TUV) radiation modelled sunlight for the 2025 summer solstice in Vancouver, BC, was 774 W m^{-2} , a value from the integrated irradiance over the same wavelength range. This simulated sunlight value is higher than that of the UBC and Ircelyon photoreactors, but lower than the UCD photoreactor, representing a need to quantify the approximate sunlight equivalents for each photoreactor 390 (Sec. 3.2.4).

3.2.3 Spectral range of wavelengths

The spectral range of wavelengths and their peak intensity are also important considerations for interpreting photochemical results. The Ircelyon photoreactor has light that extends to 285 nm, a lower threshold than the simulated sunlight from the TUV model (Fig. 3b). The UBC photoreactor configurations had UVA bulbs (348–405 nm), and UVA+UVB bulbs (300–405 nm), 395 with some additional irradiance at longer wavelengths due to fluorescence from the UVB bulbs. The UBC spectral profiles differed from the broad distribution of natural sunlight, with implications for extrapolating to the real atmosphere (Fig. 3b). Normalized photon fluxes showed similar spectral shapes for the xenon lamp setups at UCD and Ircelyon (Fig. 3b), suggesting consistency in the emission characteristics despite differences in absolute intensity. Based on differences in spectral range of the different light sources, we also explored the possible quantum yield dependence on wavelength in section 3.3.8.

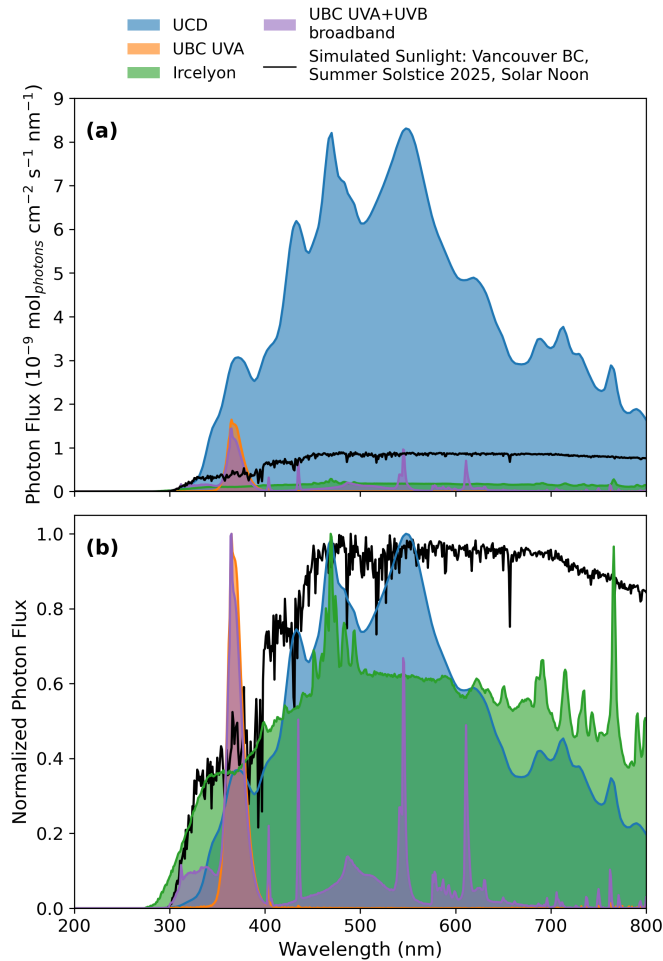


Figure 3. Irradiance measurement of photoreactor setups, showing a) Photon flux quantified using 2-nitrobenzaldehyde actinometry ($\text{mol}_{\text{photons}} \text{ cm}^{-2} \text{ s}^{-1} \text{ nm}^{-1}$, average of triplicate actinometry experiments) and b) normalized to peak irradiance. UCD is shown in blue, Ircelyon in green, and UBC in orange (UVA only) and purple (UVA+UVB broadband). Sunlight was simulated from the NCAR quick TUV calculator (https://www.acom.ucar.edu/Models/TUV/Interactive_TUV/) for solar noon on the summer solstice of 2025 in Vancouver, British Columbia (see section 3.2.4 for model details).

400 3.2.4 Rate of light absorbance equivalent hours of sunlight

To estimate the equivalent hours of sunlight experiences by the samples in each photoreactor, we compared rates of light absorbance by photosensitizers in each four photoreactor configurations to conditions under natural sunlight. The conversion factor, calculated using Eq. 16, represents the number of hours of solar exposure at 5 km altitude over Vancouver, Canada (a representative mid-tropospheric location), required to match 1 h of irradiation in a given photoreactor.



405 Equivalent hours of sunlight were determined for perinaphthenone, lignin, and juglone, based on rates of light absorbance from 2-nitrobenzaldehyde actinometry (Table 2). Consistent with our observed photon fluxes (Sec. 3.2.2), the UCD photoreactor had the highest effective light intensity with conversion factors of 5.0 to 7.1 (Table 2). In contrast, the Ircelyon photoreactor yielded the lowest values, with less than 0.3 h of natural sunlight for each hour in the photoreactor, consistent with a weaker irradiance. The UBC photoreactor setups had intermediate conversion factors, ranging from 0.23 to 0.72. These trends reflect
410 differences in both total irradiance and spectral overlap with the absorbance features of the photosensitizers, highlighting the need to characterize and report spectral irradiance, light intensity, and action spectra for each illumination system.

Table 2. Rate of light absorbance equivalent hours of sunlight for photosensitizers with atmospherically relevant moieties for an hour in each photoreactor setup calculated according to equation 16. Rates of light absorbance for photoreactors were calculated from 2-nitrobenzaldehyde actinometry, and are the mean value of triplicate experiments.

Sensitizer	UBC UVA (h)	UBC UVA+UVB broadband (h)	UCD (h)	Ircelyon (h)
Perinaphthenone	0.72	0.67	6.3	0.26
Lignin	0.45	0.60	5.0	0.29
Juglone	0.23	0.29	7.1	0.24

3.3 Quantifying $^1\text{O}_2^*$ Production

3.3.1 Measuring $^1\text{O}_2^*$ using furfuryl alcohol as a probe

We used furfuryl alcohol as a probe to measure steady-state $^1\text{O}_2^*$ concentrations indirectly (Haag et al., 1984; Appiani et al.,
415 2017). To quantify $^1\text{O}_2^*$ using this method, furfuryl alcohol must display pseudo-first order kinetics as a function of irradiation time (Figures S2 - S7). This linearity is necessary, as a deviation indicates that $^1\text{O}_2^*$ is no longer under steady-state conditions and other sources and sinks of $^1\text{O}_2^*$ are likely contributing to furfuryl alcohol's decay. Furthermore, deviations from pseudo-first-order kinetics can also be observed for longer irradiation times and weak light sources. To account for these deviations, we have previously suggested removing furfuryl alcohol time points resulting in a change in slope greater than 25% (Borduas-
420 Dedekind et al., 2024).

When using a chemical probe to determine $^1\text{O}_2^*$, all possible sinks of the probe need to be considered and accounted for. These sinks include photolysis, light screening, reactivity with other oxidants such as $\cdot\text{OH}$, and reactivity with other molecules and excited state photosensitizers (see Sec. 3.3.2). For example, a dark control will confirm the lack of reactivity between the photosensitizer and the probe in the absence of light (Fig. S1). Additionally, correcting observed decays of the probe for light screening according to Eq. 4 is necessary to account for any heterogeneity of chromophores in the sample and particularly due to concentrated and coloured samples. In our case, the screening factors were optimized to be close to 1 to specifically avoid screening (Tables S1-S4). Furthermore, to account for $\cdot\text{OH}$ reactivity with furfuryl alcohol, we recommend adding an $\cdot\text{OH}$ trap such as isopropanol to the solution (Bogler et al., 2022; Borduas-Dedekind et al., 2024). Alternatively, $\cdot\text{OH}$ can be quantified explicitly with a probe such as benzoic acid (Klein et al., 1975) or terephthalic acid (Manfrin et al., 2019). Manfrin



430 et al. (2019) found that $\cdot\text{OH}$ accounted for up to 32% of the observed furfuryl alcohol loss under 311 nm irradiation, but only up to 2% under 365 nm irradiation, highlighting the importance of quenching $\cdot\text{OH}$ or accounting for probe loss from $\cdot\text{OH}$ in the presence of UVB light.

Yellow impurities in furfuryl alcohol can also influence the reaction kinetics and the absorbance of the sample in the UVA region (Fig. S12). These impurities can contribute to the direct photodegradation of furfuryl alcohol by 3.1%, as shown in Fig. 435 S13 (Marchisio et al., 2015; Maizel et al., 2017). To limit this issue, stock solutions should be stored at 4 °C, and in dark environments (Ossola et al., 2021). Overall, using a probe such as furfuryl alcohol is an indirect method of quantification but does lend itself readily to high throughput experiments of atmospheric sample extracts.

3.3.2 Control experiments for ${}^3\text{C}^*$ reacting with furfuryl alcohol

440 Removing oxygen by bubbling with N_2 from sample solutions is an important control for verifying that the ${}^3\text{C}^*$ of the photosensitizer did not react with furfuryl alcohol at a competitive rate, which is the case for the the photosensitizing molecules used in our photoreactor intercomparison (Fig. S2, S3). However, we found that excited states of atmospherically relevant nitroanisoles (Xu et al., 2022), can react with furfuryl alcohol in the absence of O_2 leading to a ${}^1\text{O}_2^*$ false positive (Fig. S14). Nitrogen-containing compounds are ubiquitous in organic aerosols and have been found in wildfire smoke and $\text{PM}_{2.5}$ filters (Xu et al., 2018; Li et al., 2025b; Zheng et al., 2023; Fleming et al., 2020), highlighting the importance of conducting this 445 control experiment for the atmospheric context.

Furthermore, previous studies have used the kinetic solvent isotope effect as a diagnostic tool to assess the decay of furfuryl alcohol from oxidants other than ${}^1\text{O}_2^*$ (Davis et al., 2018; Lyu et al., 2023). The kinetic solvent isotope effect relies on the difference in the deactivation of ${}^1\text{O}_2^*$ in H_2O (3.5 μs , (Bregnøj et al., 2016)) and in D_2O (67 μs , (Nonell and Flors, 2016)). Although not conducted in our intercomparison study, kinetic solvent isotope effect experiments can be a useful diagnostic tool 450 to quantify the furfuryl alcohol from oxidants other than ${}^1\text{O}_2^*$.

3.3.3 Calculation of quantum yields via absolute and relative methods

455 There are two approaches to calculate a quantum yield. There is an absolute method, $\Phi_{\text{O}_2^*}^{\text{dir}}$, which relies on chemical actinometry and is measured for instance by 2-nitrobenzaldehyde or p-nitroanisole/pyridine according to Eq. 9 and used to generate Fig. 4c. In addition, there is a relative method, $\Phi_{\text{O}_2^*}^{\text{r}}$, which uses a reference photosensitizer such as perinaphthenone along with Eq.10. This method requires that a solution of perinaphthenone be run side by side with the samples in a multi-sample holder and captures changes in photon flux throughout the irradiation experiment.

For this intercomparison study, we ran both sets of experiments to evaluate the differences between the absolute and relative methods. Values between the two methods ($\Phi_{\text{O}_2^*}^{\text{dir}}$ vs $\Phi_{\text{O}_2^*}^{\text{r}}$) were consistently 15% within eachother for all sensitizers (Tables S1 - S4). Agreement between these methods is expected and supports the stability of the lights sources in all four experimental 460 setups (Table S5). Chemical actinometry has the advantage of providing both the photon flux and the corresponding quantum yield (Eq. 9), while the relative method only provides quantum yields (Eq. 10). Applying both approaches at the onset of a study can provide a consistency check to identify systematic biases in the light distribution and actinometry based quantification



within the photoreactor. Nevertheless, previous aqueous environmental studies of $^1\text{O}_2^*$ have favoured the use of actinometry over reference photosensitizer to quantify $^1\text{O}_2^*$ quantum yields (24 studies to 4 studies, reported by Ossola et al. (2021)).

465 **3.3.4 $^1\text{O}_2^*$ Quantum Yield from the probe method**

Rates of light absorbance and $^1\text{O}_2^*$ steady-state concentrations differed by several orders of magnitude across the different laboratories (Fig. 3). We attribute this range specifically to the photon flux of the light source; the more powerful the source, the higher the rate of absorbance and the higher the $^1\text{O}_2^*$ concentrations (Fig. 4 a,b). Despite these order of magnitude differences in R_{abs} and $[^1\text{O}_2^*]_{\text{ss}}$, the apparent quantum yield, $\Phi_{^1\text{O}_2^*}$, for Rose Bengal and for perinaphthenone were consistent and reproducible 470 across photoreactors and aligned with literature values (Schmidt et al., 1994; Wilkinson et al., 1993) (Fig. 4c). This result suggests that normalizing $^1\text{O}_2^*$ production to R_{abs} effectively accounted for differences in light intensity for Rose Bengal and perinaphthenone.

On the other hand, lignin and juglone deviated from this pattern: higher R_{abs} did not always correspond to higher $[^1\text{O}_2^*]_{\text{ss}}$, resulting in lower quantum yields in xenon lamp photoreactors (UCD & Ircelyon) and higher quantum yields in UV bulb 475 photoreactors (UBC). This result was unexpected. For juglone, we also noticed that the strongest light source at UCD (Figure 4a) led to the smallest $\Phi_{^1\text{O}_2^*}$ (Figure 4c left). Clearly, normalizing $[^1\text{O}_2^*]_{\text{ss}}$ by the R_{abs} was not effective for comparing juglone $\Phi_{^1\text{O}_2^*}$ across our setups. This trend was also observed for lignin to a lesser extent (Figure 4c, left), begging the question why these sensitizers are not behaving as expected. We reasoned that these differences had a likely root cause in the light source, and we further investigated their wavelength dependence.

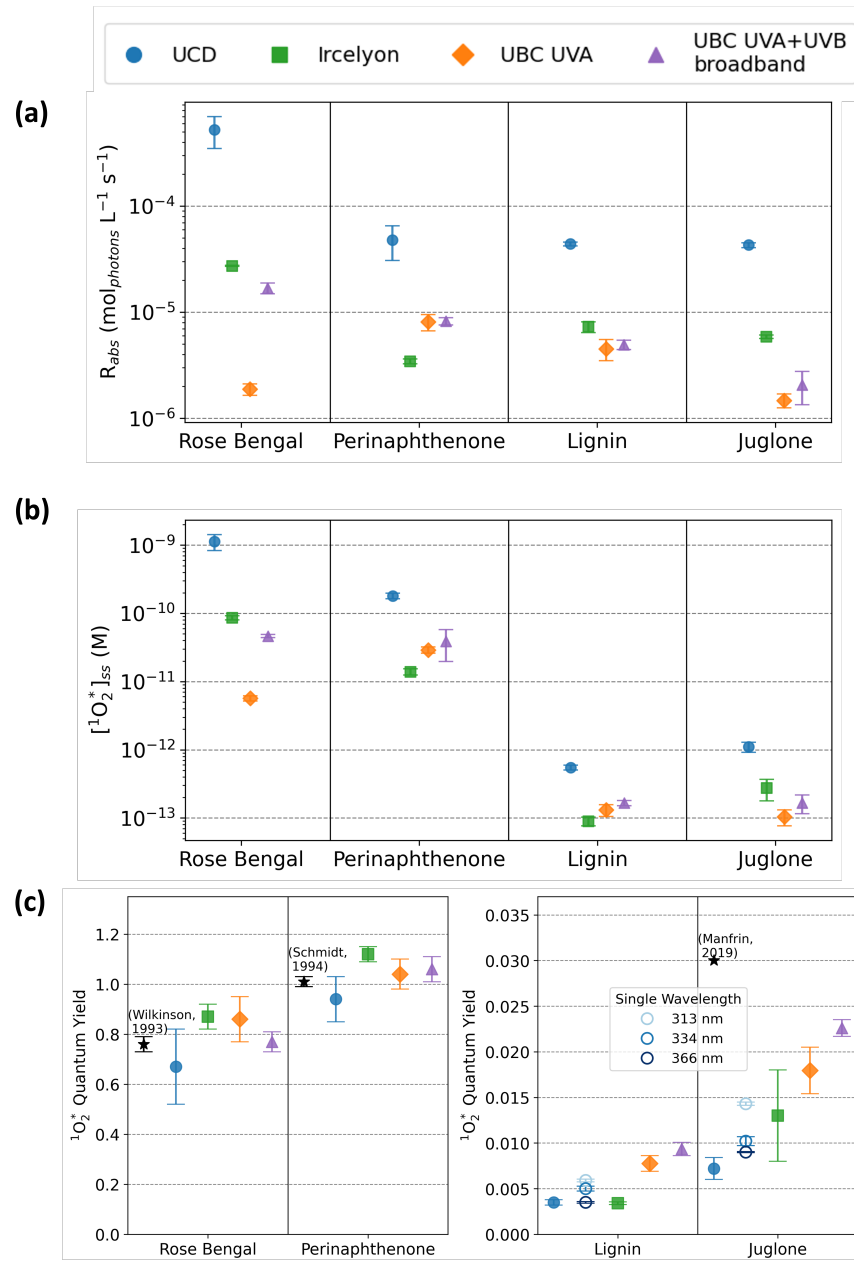


Figure 4. $^1\text{O}_2^*$ formation parameters for each photosensitizer and photoreactor setup. Panel a) is the rate of light absorbance for each photosensitizing molecule in each photoreactor setup in ($\text{mol}_{\text{photons}} \text{ L}^{-1} \text{ s}^{-1}$) (log scale), b) is $^1\text{O}_2^*$ steady-state concentrations (M) (log scale), and c) is the resulting $^1\text{O}_2^*$ quantum yield values, calculated using equation 9, separated into efficient photosensitizers (Rose Bengal and perinaphthenone, left panel) and less efficient photosensitizers (juglone and lignin, right panel), with adjusted y-axes. Previously reported values, when available, are plotted as black stars. Previously reported quantum yield values in water are 0.76 ± 0.02 for Rose Bengal (Wilkinson et al., 1993), 1.01 ± 0.03 (Schmidt et al., 1994) for perinaphthenone, and 0.03 for juglone (excitation wavelength centred at 365 nm) (Manfrin et al., 2019). Single wavelength experiments to test for the wavelength dependence of $\Phi_{^1\text{O}_2^*}$ (Sec. 2.8) for lignin and juglone are shown as open circles (conducted at 313 nm, 334 nm, and 366 nm).



480 **3.3.5 Wavelength-dependency of quantum yields**

¹O₂^{*} quantum yields decrease with increasing wavelength in surface water samples (Partanen et al., 2020), and for juglone (Manfrin et al., 2019). In this study, for both lignin and juglone, lower wavelengths led to an increase in $\Phi_{1\text{O}_2^*}$ (Fig. 4, S20). One possible explanation is that the photosensitizer with high energy photons results in higher singlet to triplet intersystem crossing rates, k_{ISC} (Drozd et al., 2024), which is the precursor step to forming ¹O₂^{*}. This increase in intersystem crossing rate 485 has been observed for a range of aromatic molecules relevant to the atmosphere (Valiev et al., 2025), and is consistent with the observed increase in $\Phi_{1\text{O}_2^*}$ here. While a quantitative relationship between photon energy and increasing $\Phi_{1\text{O}_2^*}$ does not exist, there is clear evidence for wavelength-dependent quantum yields for photosensitizing molecules with atmospherically relevant moieties and samples (Partanen et al., 2021; Manfrin et al., 2019). For this reason, reporting the irradiance spectrum 490 is necessary for the interpretation of $\Phi_{1\text{O}_2^*}$ values. This wavelength sensitivity introduces a measurement-dependent bias when different light sources are used and must therefore be treated as a methodological constraint.

Due to wavelength dependencies, results obtained using narrow or single wavelength irradiation can be difficult to reliably extrapolate to the broader solar spectrum. Accordingly, using sunlight-mimicking irradiation sources are best recommended. Anton et al. (2024) recommended that, to obtain more accurate measurements, researchers should: 1) select a chemical actinometer that absorbs light in the same spectral region as the compound of interest, and 2) minimize inner filter effects by 495 employing optically transparent solutions.

3.3.6 ¹O₂^{*} quantum yield from phosphorescence data

The phosphorescence measurement of ¹O₂^{*} is a direct spectroscopic technique where a sensitizer is excited at 355 nm and the relaxation of ¹O₂^{*} to the ground state is detected at 1270 nm (Kabanov et al., 2019). This technique does not suffer from interferences outlined for the indirect probe method (Sec. 3.3.1 & 3.3.2). However, it does not provide information on ¹O₂^{*} 500 reactivity (i.e. no information on k_{obs}) that chemical probe methods provide (Partanen et al., 2020; Schweitzer and Schmidt, 2003).

We also used 4-nitrophenol and nitroanisoles as additional sensitizers in our comparison of the probe and spectroscopic methods. Interestingly, lignin, 2-nitroanisole, 4-nitroanisole and 4-nitrophenol had ¹O₂^{*} quantum yields of 0 in the phosphorescence set up, but measurable ¹O₂^{*} quantum yields using the chemical probe method (Table 3). This discrepancy is hypothesized 505 to be due to the detection limit of the photomultiplier tube in the phosphorescence set up. The comparison of the results and the differences observed among the photosensitizers supports the conclusion that the direct phosphorescence method, despite its high specificity, may lack sufficient sensitivity to detect ¹O₂^{*} emission for photosensitizers with low ¹O₂^{*} quantum yields. For juglone, a phosphorescence signal was detected due to its higher ¹O₂^{*} quantum yield. Discrepancies between the methods 510 is hypothesized to be due to an observed wavelength dependence on ¹O₂^{*} quantum yield from the single wavelength laser used (355 nm) in phosphorescence experiments (Sec. 3.3.4). As for 3-nitroanisole's high quantum yield by both the chemical probe and direct phosphorescence methods, the unique meta position of the methoxy and the nitro substituents has been suggested



to lead to an excited state through a low lying π, π^* triplet state (Mir et al., 1998), which is in fact consistent with a high ${}^1\text{O}_2^*$ quantum yield (Schweitzer et al., 2003; Gollnick et al., 1970).

Table 3. ${}^1\text{O}_2^*$ quantum yields ($\Phi_{{}^1\text{O}_2^*}$) calculated from equation 10 for photosensitizers: Rose Bengal, Lignin, Juglone, 2-nitroanisole, 3-nitroanisole, 4-nitroanisole, and 4-nitrophenol, measured by chemical probe (FFA) and direct phosphorescence (1270 nm).

Sensitizer	Chemical Probe (UBC UVA)	Direct Phosphorescence (1270 nm)
	$(\Phi_{{}^1\text{O}_2^*}, \%)$	$(\Phi_{{}^1\text{O}_2^*}, \%)$
Rose Bengal	83 ± 10.0	78.1 ± 10.0
Lignin	0.75 ± 0.07	0
Juglone	1.73 ± 0.22	5.3 ± 1.7
2-nitroanisole	1.25 ± 0.18	0
3-nitroanisole	34.4 ± 2.14	24.3 ± 4.8
4-nitroanisole	8.83 ± 1.07	0
4-nitrophenol	0.8 ± 0.01	0

3.3.7 Role of dissolved oxygen

515 Discrepancies between phosphorescence and chemical probe methods can be attributed to different factors. For Rose Bengal, discrepancies between the methods (83% using chemical probe, and 78% using phosphorescence, Table 3) could be due to differences in dissolved O_2 . To test this hypothesis, we estimated the partial pressure of O_2 at the location of the measurement, used O_2 's Henry's Law constant to estimate the amount of dissolved O_2 and then calculated the fraction of triplets quenched by O_2 using the constant for the deactivation triplets, k_d^T from Erickson et al. (2018) and calculating ($k_{\text{O}_2}[\text{O}_2]$). This approach
520 led to values of $p_{\text{O}_2} = 0.18$ atm and 0.21 atm for Calgary (1113 m elevation) where the phosphorescence measurements were made and for Vancouver (95 m elevation) where the chemical probe measurements were made, respectively. We then used the Henry's law constant for O_2 at $k^{\circ\text{H}} = 0.0013 \text{ M atm}^{-1}$ (NIST). Next, Erickson et al. (2018) reported $k_{\text{O}_2} = 8.9 \times 10^8 \text{ M}^{-1} \text{ s}^{-1}$ and $k_d^T = 9.0 \times 10^4 \text{ s}^{-1}$ for the average of 7 natural-water samples. This calculation led to ${}^3\text{C}^*$ deactivation pathways yields $k_{\text{O}_2}[\text{O}_2]$ that were 2.8 times larger than k_d^T in Vancouver, and 2.5 times larger in Calgary. In other words, a lower p_{O_2} would
525 result in a lower $\Phi_{{}^1\text{O}_2^*}$, according to Eq. 8, consistent with the quantum yield for Rose Bengal that we reported in Table 3.

For the nitroanisole compounds, lower ${}^1\text{O}_2^*$ quantum yields were obtained during the phosphorescence measurements compared to the chemical probe quantification. Specifically, a decrease in $\Phi_{{}^1\text{O}_2^*}$ of 1.2%, 10.1%, and 8.8% was observed for 2-nitroanisole, 3-nitroanisole, and 4-nitroanisole respectively. We hypothesize that this discrepancy can be attributed to the reactivity of the ${}^3\text{C}^*$ of the nitroanisoles with furfuryl alcohol observed in the absence of O_2 (Sec. 3.3.1, Fig. S14). The proposed mechanism is a substitution reaction involving the nitro group on nitroanisole and the alcohol on furfuryl alcohol, proceeding under light with wavelengths greater than 300 nm in water (Dulin and Mill, 1982). In these cases, furfuryl alcohol



is not a suitable probe for $^1\text{O}_2^*$ in the presence of nitro groups, which are particularly prevalent in BrC and the atmospheric chemistry context.

3.3.8 Photochemical action regions

535 Photochemical action spectra represent rates of light absorbance as a function of wavelength, and provide insights into the specific wavelength regions that drive photochemical reactions. Rose Bengal exhibited a strong absorbance peak at 549 nm in water, which dominated its photochemical action spectra in all photoreactors except the UBC UVA setup, where no irradiance was present at this wavelength (Fig. 5a). Remarkably, despite this difference, $\Phi_{^1\text{O}_2^*,\text{RB}}$ remained comparable across all setups, indicating no wavelength dependence. Perinaphthenone action regions also differed, with xenon lamp photoreactors displaying 540 broader regions (e.g. 294–480 nm at Ircelyon) and narrower regions in the UV photoreactor setups (e.g. 348–405 nm for UBC UVA) (Fig. 5b). The differences in action regions did not lead to an observed difference in $\Phi_{^1\text{O}_2^*,\text{PN}}$, suggesting that the quantum yield is independent of wavelength, and effectively normalizes R_{abs} and $^1\text{O}_2^*$ production.

545 The juglone action spectra peaked at longer wavelengths in xenon lamps (433 nm at UCD, 421 nm at Ircelyon), where lower $\Phi_{^1\text{O}_2^*,\text{Juglone}}$ values were observed (Fig. 4c). UBC photoreactors showed peaks at 365 nm, with the UVA+UVB broadband setup extending further into the UV (down to 304 nm) and producing the highest $\Phi_{^1\text{O}_2^*,\text{Juglone}}$, consistent with increased excitation by higher energy photons (Fig. 5d). A similar trend was observed for lignin; increased contributions from high energy photons in the UBC UVA and UVA+UVB broadband systems led to higher $\Phi_{^1\text{O}_2^*,\text{Lignin}}$ compared to the UCD and Ircelyon xenon lamp setups. This general trend is consistent with previous studies for quantum yields of photodegradation (Anton et al., 2024).

550 An important consideration in the analysis of photochemical action regions is the potential for light scattering in absorbance measurements. Scattering of light in UV-Vis absorbance measurements should be considered as a source of uncertainty in absorbance measurements, even if samples were filtered (Sec. S8, Fig. S15, S16) (Bieber et al., 2024). Scattering from nanoparticles is particularly challenging, and can artificially increase rates of light absorbance. We therefore recommend that future studies recognize and discuss the potential influence of light scattering when interpreting light absorbance measurements. Sample absorbance should be measured before and after filtering with a $0.22\ \mu\text{m}$ membrane filter. In this work, we also conducted 555 a sensitivity analysis of the light scattering from nanoparticles (Sec. S8). Particle concentrations below the detection limits of nanoparticle tracking analysis or dynamic light scattering can produce errors over 100% in calculated absorbance rates (Fig. S17). These findings indicate that calculated rates of light absorbance, and consequently, $^1\text{O}_2^*$ quantum yields, may be sensitive to scattering artifacts and introduce an additional source of uncertainty.

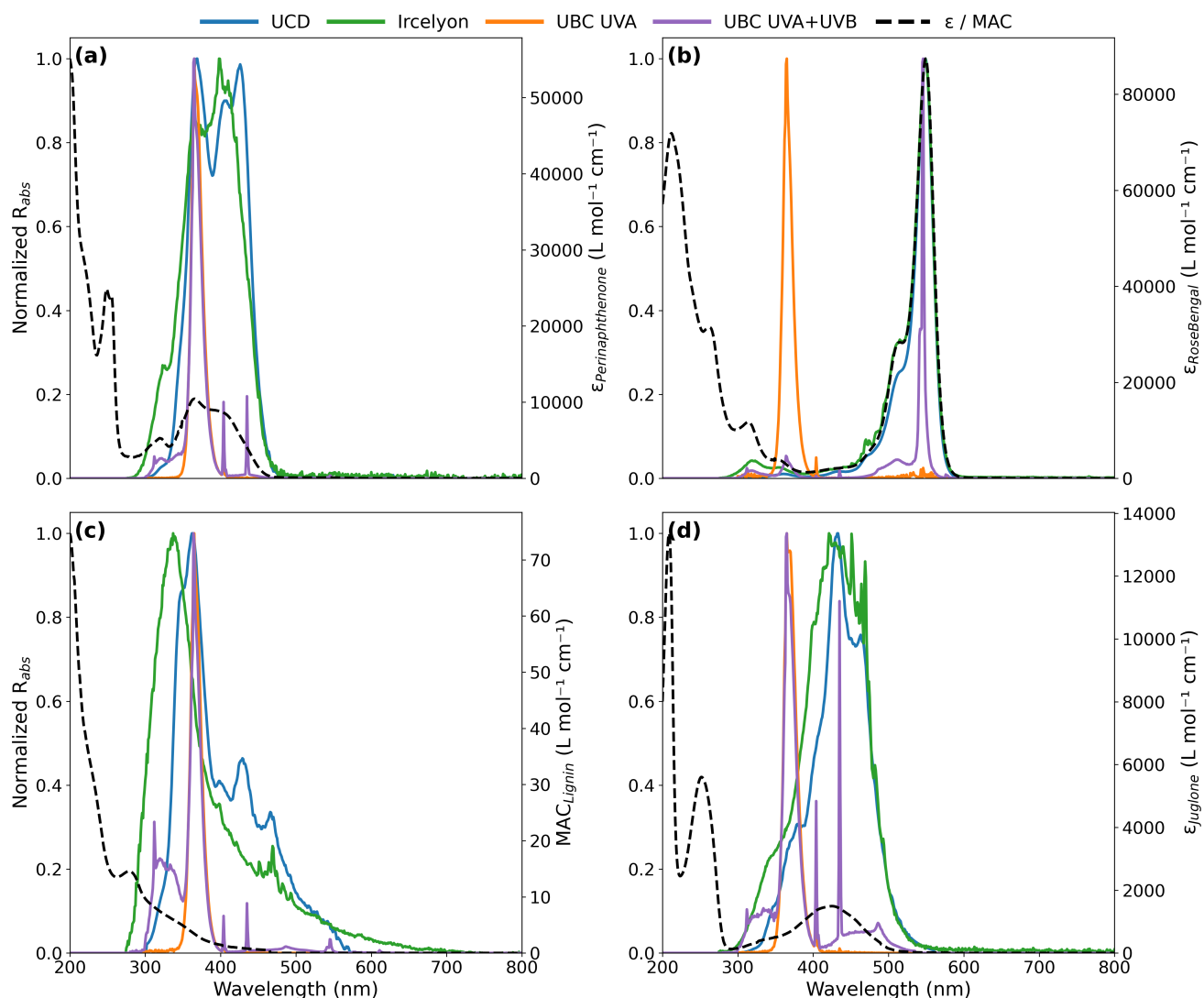


Figure 5. Normalized to peak (i.e., peak value = 1) wavelength-distributed rate of light absorbance for a) perinaphthenone, b) Rose Bengal, c) lignin, and d) juglone for all four photoreactor setups from three different labs (UCD, Ircelyon, UBC). Molar absorption coefficients are shown as black dashed lines and correspond to the right y-axis for all compounds. Wavelength-distributed rate of light absorbance is calculated using the form of equation 1 prior to summation.



4 Recommendations

560 Reproducible and comparable quantification of $^1\text{O}_2^*$ in atmospheric systems requires attention to experimental design and data analysis. Previously measured R_{abs} for environmental samples are on the order of 10^{-6} to 10^{-5} mol_{photons} L⁻¹ s⁻¹ for fog water samples (Kaur and Anastasio, 2017) and for PM extracts in multiple studies (Bogler et al., 2022; Kaur et al., 2019b; Petersen-Sonn et al., 2025; Ma et al., 2023a). $[^1\text{O}_2^*]_{\text{SS}}$ measured from particulate matter (PM) extracts using chemical probe-based methods have been reported in the range of 10^{-14} to 10^{-12} M and depend strongly on the extract concentration (Kaur et al., 2019a; Leresche et al., 2021; Lyu et al., 2023; Ma et al., 2024; Manfrin et al., 2019; Bogler et al., 2022).

565 However, direct comparisons of R_{abs} and $[^1\text{O}_2^*]_{\text{SS}}$ across different studies are complicated by differences in photoreactor light output, which dictate the magnitude of these parameters. $^1\text{O}_2^*$ quantum yield ($\Phi_{^1\text{O}_2^*}$) offers a more comparable metric, as it normalizes for photon flux and photosensitizer concentration. Previously reported $\Phi_{^1\text{O}_2^*}$ values from atmospheric samples range from 0.002 to up to 0.19, highlighting the large range of $\Phi_{^1\text{O}_2^*}$ values for more complex systems (Petersen-Sonn et al., 570 2025; Ma et al., 2023a; Kaur et al., 2019b; Bogler et al., 2022; Manfrin et al., 2019; Ma et al., 2024; Lyu et al., 2023).

Based on this intercomparison, we make the following recommendations to improve the reproducibility and interpretation of atmospheric $^1\text{O}_2^*$ measurements across experimental setups:

1. **Considering wavelength dependence:** Excited state oxidant studies should explicitly report the irradiation wavelengths used. At a minimum, spectrophotometer measurements and photochemical action spectra should be included. Without this information, it can be difficult to interpret results across different studies or to evaluate the influence of wavelength-dependence on reported apparent quantum yields.
2. **Chemical probe concentration:** We recommend using concentrations of furfuryl alcohol equivalent to less than 1% of the sensitizers, to ensure that the sink of $^1\text{O}_2^*$ to the probe remains negligible. Ossola et al. (2021) recommends a general rule of $[\text{FFA}]_0 < 145 \mu\text{M}$ to satisfy this condition. If the probe concentration is greater than this threshold, then quenching will need to be accounted for (De Laurentiis et al., 2013; Frimmel et al., 1987).
3. **Control and report the temperature of photoreactor:** We recommend that photoreactor setups be temperature controlled within a minimum range of 20–25 °C. This recommendation is based on experimental evidence presented here (Fig. S18, S19) as well as evidence presented in Appiani et al. (2017). These authors demonstrated temperature-dependence in both the deactivation rate of $^1\text{O}_2^*$ in water and the reaction rate of furfuryl alcohol with $^1\text{O}_2^*$.
4. **Light scattering considerations:** When working with particulate matter extracts, solutions may contain insoluble material which can scatter light during a UV/Vis spectrometry measurement. Thus, the impact of light scattering should be considered when calculating rates of light absorbance, as scattering can artificially increase apparent absorbance by accounting for scattered light.
5. **Control experiments:** Experiments should include a sample without a photosensitizer to evaluate direct chemical probe decay, and a sample without light to assess probe degradation in the dark (Fig. S1). Adding an $\cdot\text{OH}$ radical trap is also



595

important to mitigate furfuryl alcohol decay due to other oxidants. Additionally, experiments conducted in the absence of oxygen are necessary to determine whether the chemical probe reacts directly with the $^3\text{C}^*$, particularly in atmospheric contexts where nitroaromatic compounds can react with furfuryl alcohol (Sec. 3.3.1, Fig. S14). Experiments using deuterated water can test for kinetic solvent isotope effects, providing additional confirmation that furfuryl alcohol decay arises exclusively from $^1\text{O}_2^*$. Incorporating these control experiments ensures that measured probe decay can be accurately attributed to the intended reactive species, enhancing the reliability and intercomparability of $^1\text{O}_2^*$ quantification.

5 Building a new photoreactor

600

Here, we weigh the advantages and disadvantages of photoreactor setups used across atmospheric chemistry labs to consider the features of an ideal photoreactor. The ideal photoreactor would have 1) an irradiance spectrum that reproduces the solar spectrum such as a xenon lamp, 2) a temperature control across a wide range, and 3) a system for high throughput samples. As highlighted in section 3.2, to extrapolate laboratory measurements to the atmosphere, the use of natural sunlight is an advantage. Xenon lamps replicate the relevant wavelength distribution of the solar spectrum well, but suffer from low throughput limitations (Sec. 3.1.2) because xenon lamps are point sources of light and thus incompatible with cylindrical photoreactors which require multiple light sources. Using multiple bulb types, or LED lights (Wu et al., 2021), in a photoreactor such as the Rayonet do not cover all wavelengths in the photoreactor but offer a higher throughput setup. There are photoreactors on the market that act as incubators, (Anton et al., 2024) but they may not have the same photon flux penetrate all samples uniformly. The intercomparison work presented here illustrates the trade offs between spectral accuracy, photon flux intensity, and throughput, offering guidance for designing, optimizing, and validating new photoreactor setups depending on the research question.

610

6 Atmospheric implications

615

Forest fires release chromophoric species to the atmosphere, highlighting the importance of studying photochemically-generated oxidants, including $^3\text{C}^*$ and $^1\text{O}_2^*$, which can drive multiphase atmospheric chemistry. Recent laboratory and field studies have demonstrated that steady-state concentrations of $^1\text{O}_2^*$ in atmospheric waters and aerosol liquid water often exceed those of $\cdot\text{OH}$ by two to three orders of magnitude, particularly in particulate phases enriched in BrC (Ma et al., 2023a; Manfrin et al., 2019). Under these conditions, $^1\text{O}_2^*$ can dominate over $\cdot\text{OH}$ in the oxidation of specific compound classes, including N-containing compounds and S-containing compounds. (Manfrin et al., 2019) $^1\text{O}_2^*$ is also the dominant oxidant over $^3\text{C}^*$ and $\cdot\text{OH}$ for amino acids and carboxamides (Petersen-Sonn et al., 2025), thereby impacting organic aerosol aging, aqueous SOA formation, and BrC evolution.

620

Despite its growing importance, quantitative comparisons of $^1\text{O}_2^*$ across studies remain challenging due to methodological differences in probe and actinometer selection, light source, light normalization, and competing sinks for the probe, the sensi-



tizer and $^1\text{O}_2^*$. Consequently, variability in reported $^1\text{O}_2^*$ concentrations can span orders of magnitude even for similar particle types, limiting our ability to select a concentration or quantum yield as inputs for constraining models. Nevertheless, Zhang et al. (2024) parameterized $^3\text{C}^*$ and $^1\text{O}_2^*$ as functions of dissolved organic carbon and light absorption to predict secondary 625 organic aerosol formation from wildfire smoke phenols. The authors highlighted how the uncertain in $^1\text{O}_2^*$ steady-state concentrations was a limitation in their study. The intercomparison presented here addresses this gap by systematically evaluating commonly used $^1\text{O}_2^*$ quantification approaches under controlled yet atmospherically relevant conditions. By establishing this best-practice guide for probe choice, control experiments, calibrations, actinometry, wavelength-dependent quantum yields and 630 and uncertainty reporting, this work enables more robust inter-study comparisons and facilitates integration of $^1\text{O}_2^*$ chemistry into multiphase chemical models.

Furthermore, photochemical experiments for quantifying $^1\text{O}_2^*$ are conducted in bulk solutions and are therefore not representative of concentrated organic aerosols. Kaur et al. (2019b); Ma et al. (2021) have estimated that $^1\text{O}_2^*$ is likely underestimated in particulate matter as the concentration of chromophores increases, despite adding organic matter as sinks for $^1\text{O}_2^*$. There is also an ongoing need to identify unique sensitizers relevant for the atmosphere such as nitrophenols in BrC, (Fleming et al., 2020; 635 Siemens et al., 2023) to further understand the drivers of excited state oxidants in aerosols. In addition, Chang et al. (2025) used structure-activity relationships and machine learning approaches to predict $^3\text{C}^*$ and $^1\text{O}_2^*$ and identified photosensitizer properties, intersystem crossing yields and triplet-state energies as sources of uncertainty. We hope that our intercomparison study addresses this need by harmonizing methodologies for quantifying $^1\text{O}_2^*$, enabling closer integration between predictive 640 photosensitizer models and multiphase atmospheric chemistry simulations.

640 *Data availability.* All data collected and used in this study are available in the SI (Tables S1 – S4)

645 *Author contributions.* NBD, EAPS, & LMDH conceptualized the study with contributions from CG and CA. KJG & CS conducted measurements at UBC, LMDH conducted measurements at UC Davis, and EAPS & ZG conducted measurements at Irceylon. KJG conducted the phosphorescence measurements at U of Calgary with support from NMO and BH. KJG and NBD wrote the manuscript with contributions from all authors.

Competing interests. There are no conflicts to declare.

Acknowledgements. The authors thank Benjamin Herring in the shared instrument facility at UBC for their support with the HPLC and UV-Vis instruments. The authors acknowledge preliminary experiments by Chloé Arthozoul and Denise Chew on some photosensitizers



under different light conditions. This research was funded by the University of British Columbia, including a 4-Year Fellowship for KJG,
650 and NSERC. This research was supported through computational resources and services provided by Advanced Research Computing at the
University of British Columbia. The authors also acknowledge support from the French National Research Agency under the grant agreement
SENSOX (ANR-22-CE01-0023), the University of Lyon 1, and the US National Science Foundation (Grant # 2220307).



References

Akherati, A., He, Y., Garofalo, L. A., Hodshire, A. L., Farmer, D. K., Kreidenweis, S. M., Permar, W., Hu, L., Fischer, E. V., Jen, C. N.,
655 Goldstein, A. H., Levin, E. J. T., DeMott, P. J., Campos, T. L., Flocke, F., Reeves, J. M., Toohey, D. W., Pierce, J. R., and Jathar, S. H.: Dilution and photooxidation driven processes explain the evolution of organic aerosol in wildfire plumes, *Environmental Science: Atmospheres*, 2, 1000–1022, <https://doi.org/10.1039/D1EA00082A>, publisher: RSC, 2022.

Albinet, A., Minero, C., and Vione, D.: Photochemical generation of reactive species upon irradiation of rainwater: Negligible photoactivity of dissolved organic matter, *Science of The Total Environment*, 408, 3367–3373, <https://doi.org/10.1016/j.scitotenv.2010.04.011>, 2010.

660 Anastasio, C. and McGregor, K. G.: Chemistry of fog waters in California's Central Valley: 1. In situ photoformation of hydroxyl radical and singlet molecular oxygen, *Atmospheric Environment*, 35, 1079–1089, [https://doi.org/10.1016/S1352-2310\(00\)00281-8](https://doi.org/10.1016/S1352-2310(00)00281-8), 2001.

Anton, L. d. B., Silverman, A. I., and Apell, J. N.: Determining wavelength-dependent quantum yields of photodegradation: importance of experimental setup and reference values for actinometers, *Environmental Science: Processes & Impacts*, 26, 1052–1063, <https://doi.org/10.1039/D4EM00084F>, publisher: The Royal Society of Chemistry, 2024.

665 Appiani, E., Ossola, R., Latch, D. E., Erickson, P. R., and McNeill, K.: Aqueous singlet oxygen reaction kinetics of furfuryl alcohol: effect of temperature, pH, and salt content, *Environmental Science: Processes & Impacts*, 19, 507–516, <https://doi.org/10.1039/C6EM00646A>, 2017.

Arakaki, T., Anastasio, C., Kuroki, Y., Nakajima, H., Okada, K., Kotani, Y., Handa, D., Azechi, S., Kimura, T., Tsuhako, A., and Miyagi, Y.: A General Scavenging Rate Constant for Reaction of Hydroxyl Radical with Organic Carbon in Atmospheric Waters, *Environ. Sci. Technol.*, 47, 8196, 2013.

670 Armarego, W. L. F. and Chai, C.: Chapter 4 - Purification of Organic Chemicals, in: *Purification of Laboratory Chemicals* (Seventh Edition), edited by Armarego, W. L. F. and Chai, C., pp. 103–554, Butterworth-Heinemann, Boston, ISBN 978-0-12-382161-4, <https://doi.org/10.1016/B978-0-12-382161-4.00004-2>, 2013.

Bieber, P., Darwish, G. H., Algar, W. R., and Borduas-Dedekind, N.: The presence of nanoparticles in aqueous droplets containing plant-derived biopolymers plays a role in heterogeneous ice nucleation, *The Journal of Chemical Physics*, 161, 094304, <https://doi.org/10.1063/5.0213171>, 2024.

675 Bogler, S., Daellenbach, K. R., Bell, D. M., Prévôt, A. S. H., El Haddad, I., and Borduas-Dedekind, N.: Singlet Oxygen Seasonality in Aqueous PM10 is Driven by Biomass Burning and Anthropogenic Secondary Organic Aerosol, *Environmental Science & Technology*, 56, 15 389–15 397, <https://doi.org/10.1021/acs.est.2c04554>, 2022.

680 Borduas-Dedekind, N., J. Gemmell, K., Madri Jayakody, M., M. Lee, R. J., Sardena, C., and Zala, S.: Singlet oxygen is produced from brown carbon-containing cooking organic aerosols (BrCOA) under indoor lighting, *Environmental Science: Atmospheres*, 4, 611–619, <https://doi.org/10.1039/D3EA00167A>, 2024.

Bregnøj, M., Westberg, M., Jensen, F., and Ogilby, P. R.: Solvent-dependent singlet oxygen lifetimes: temperature effects implicate tunneling and charge-transfer interactions, *Physical Chemistry Chemical Physics*, 18, 22 946–22 961, <https://doi.org/10.1039/C6CP01635A>, publisher: The Royal Society of Chemistry, 2016.

685 Burnett, A. I., Wiseman, C. L. S., and Styler, S. A.: Photochemical Production of Singlet Oxygen by Toronto Road Dust, *Environmental Science & Technology*, 59, 19 377–19 386, <https://doi.org/10.1021/acs.est.4c09631>, publisher: American Chemical Society, 2025.

Chang, Y., Liang, Z., Qin, Y., Zhou, L., and Chan, C. K.: Profiling the Photosensitizing Properties of Atmospheric Brown Carbon, *ACS ES&T Air*, 2, 2081–2091, <https://doi.org/10.1021/acsestair.5c00098>, publisher: American Chemical Society, 2025.



690 Cole, C. A., Carlsten, C., Koehle, M., and Brauer, M.: Particulate matter exposure and health impacts of urban cyclists: A randomized crossover study, *Environmental Health: A Global Access Science Source*, <https://doi.org/10.1186/s12940-018-0424-8>, 2018.

Cote, C. D., Schneider, S. R., Lyu, M., Gao, S., Gan, L., Holod, A. J., Chou, T. H. H., and Styler, S. A.: Photochemical Production of Singlet Oxygen by Urban Road Dust, *Environmental Science & Technology Letters*, 5, 92–97, <https://doi.org/10.1021/acs.estlett.7b00533>, 2018.

Davis, C. A., McNeill, K., and Janssen, E. M.-L.: Non-Singlet Oxygen Kinetic Solvent Isotope Effects in Aquatic Photochemistry, *Environmental Science & Technology*, 52, 9908–9916, <https://doi.org/10.1021/acs.est.8b01512>, 2018.

695 De Laurentiis, E., Buoso, S., Maurino, V., Minero, C., and Vione, D.: Optical and Photochemical Characterization of Chromophoric Dissolved Organic Matter from Lakes in Terra Nova Bay, Antarctica. Evidence of Considerable Photoreactivity in an Extreme Environment, *Environmental Science & Technology*, 47, 14 089–14 098, <https://doi.org/10.1021/es403364z>, publisher: American Chemical Society, 2013.

700 Dhaini, B., Wagner, L., Moinard, M., Daouk, J., Arnoux, P., Schohn, H., Schneller, P., Acherar, S., Hamieh, T., Frochot, C., Dhaini, B., Wagner, L., Moinard, M., Daouk, J., Arnoux, P., Schohn, H., Schneller, P., Acherar, S., Hamieh, T., and Frochot, C.: Importance of Rose Bengal Loaded with Nanoparticles for Anti-Cancer Photodynamic Therapy, *Pharmaceuticals*, 15, <https://doi.org/10.3390/ph15091093>, company: Multidisciplinary Digital Publishing Institute Distributor: Multidisciplinary Digital Publishing Institute Institution: Multidisciplinary Digital Publishing Institute Label: Multidisciplinary Digital Publishing Institute Publisher: publisher, 2022.

705 Drozd, G. T., Weltzin, T., Skiffington, S., Lee, D., Valiev, R., Kurtén, T., Madison, L. R., He, Y., and Gargano, L.: Wavelength-resolved quantum yields for vanillin photochemistry: self-reaction and ionic-strength implications for wildfire brown carbon lifetime, *Environmental Science: Atmospheres*, 4, 509–518, <https://doi.org/10.1039/D4EA00002A>, publisher: RSC, 2024.

Du, Z., He, Y., Fan, J., Fu, H., Zheng, S., Xu, Z., Qu, X., Kong, A., and Zhu, D.: Predicting apparent singlet oxygen quantum yields of dissolved black carbon and humic substances using spectroscopic indices, *Chemosphere*, 194, 405–413, <https://doi.org/10.1016/j.chemosphere.2017.11.172>, 2018.

710 Dulin, D. and Mill, T.: Development and evaluation of sunlight actinometers, *Environmental Science & Technology*, 16, 815–820, <https://doi.org/10.1021/es00105a017>, publisher: American Chemical Society, 1982.

Durantini, A. M. and Greer, A.: Interparticle Delivery and Detection of Volatile Singlet Oxygen at Air/Solid Interfaces, *Environmental Science & Technology*, 55, 3559–3567, <https://doi.org/10.1021/acs.est.0c07922>, publisher: American Chemical Society, 2021.

715 Durantini, A. M., Lapoot, L., Jabeen, S., Ghosh, G., Bipu, J., Essang, S., Singh, B. C., and Greer, A.: Tuning the 1O_2 Oxidation of a Phenol at the Air/Solid Interface of a Nanoparticle: Hydrophobic Surface Increases Oxophilicity, *Langmuir*, 39, 11 134–11 144, <https://doi.org/10.1021/acs.langmuir.3c01676>, publisher: American Chemical Society, 2023.

Erickson, P. R., Moor, K. J., Werner, J. J., Latch, D. E., Arnold, W. A., and McNeill, K.: Singlet Oxygen Phosphorescence as a Probe for Triplet-State Dissolved Organic Matter Reactivity, *Environmental Science & Technology*, 52, 9170–9178, <https://doi.org/10.1021/acs.est.8b02379>, publisher: American Chemical Society, 2018.

720 Faust, B. C. and Allen, J. M.: Aqueous-phase photochemical sources of peroxy radical and singlet molecular oxygen in clouds and fog, *Journal of Geophysical Research: Atmospheres*, 97, 12 913–12 926, <https://doi.org/10.1029/92JD00843>, 1992.

Fleming, L. T., Lin, P., Roberts, J. M., Selimovic, V., Yokelson, R., Laskin, J., Laskin, A., and Nizkorodov, S. A.: Molecular Composition and Photochemical Lifetimes of Brown Carbon Chromophores in Biomass Burning Organic Aerosol, *Atmos. Chem. Phys.*, 20, 1105, 2020.

725 Frimmel, F. H., Bauer, H., Putzien, J., Murasecco, P., and Braun, A. M.: Laser flash photolysis of dissolved aquatic humic material and the sensitized production of singlet oxygen, *Environmental Science & Technology*, 21, 541–545, <https://doi.org/10.1021/es00160a002>, publisher: American Chemical Society, 1987.



Galbavy, E. S., Ram, K., and Anastasio, C.: 2-Nitrobenzaldehyde as a chemical actinometer for solution and ice photochemistry, *Journal of Photochemistry and Photobiology A: Chemistry*, 209, 186–192, <https://doi.org/10.1016/j.jphotochem.2009.11.013>, 2010.

730 George, C., Ammann, M., D'Anna, B., Donaldson, D. J., and Nizkorodov, S. A.: Heterogeneous Photochemistry in the Atmosphere, *Chemical Reviews* (Washington, DC, United States), 115, 4218–4258, <https://doi.org/10.1021/cr500648z>, 2015.

Gianotti, E., Martins Estevão, B., Cucinotta, F., Hioka, N., Rizzi, M., Renò, F., and Marchese, L.: An Efficient Rose Bengal Based Nanoplatform for Photodynamic Therapy, *Chemistry – A European Journal*, 20, 10921–10925, <https://doi.org/10.1002/chem.201404296>, _eprint: <https://chemistry-europe.onlinelibrary.wiley.com/doi/pdf/10.1002/chem.201404296>, 2014.

735 Go, B. R., Li, Y. J., Huang, D. D., and Chan, C. K.: Aqueous-Phase Photoreactions of Mixed Aromatic Carbonyl Photosensitizers Yield More Oxygenated, Oxidized, and less Light-Absorbing Secondary Organic Aerosol (SOA) than Single Systems, *Environmental Science & Technology*, 58, 7924–7936, <https://doi.org/10.1021/acs.est.3c10199>, publisher: American Chemical Society, 2024.

Gollnick, K., Franken, T., Schade, G., and Dörhöfer, G.: Photosensitized Oxygenation as a Function of the Triplet Energy of Sensitizers*, *Annals of the New York Academy of Sciences*, 171, 89–107, <https://doi.org/10.1111/j.1749-6632.1970.tb39307.x>, _eprint: <https://onlinelibrary.wiley.com/doi/pdf/10.1111/j.1749-6632.1970.tb39307.x>, 1970.

740 Gottschalk, P., Paczkowski, J., and Neckers, D. C.: Factors influencing the quantum yields for rose bengal formation of singlet oxygen, *Journal of Photochemistry*, 35, 277–281, [https://doi.org/10.1016/0047-2670\(86\)87059-9](https://doi.org/10.1016/0047-2670(86)87059-9), 1986.

Haag, W. R., Hoigne', J., Gassman, E., and Braun, A.: Singlet oxygen in surface waters — Part I: Furfuryl alcohol as a trapping agent, *Chemosphere*, 13, 631–640, [https://doi.org/10.1016/0045-6535\(84\)90199-1](https://doi.org/10.1016/0045-6535(84)90199-1), 1984.

745 Heinlein, L. M. D., He, J., Sunday, M. O., Guo, F., Campbell, J., Moon, A., Kapur, S., Fang, T., Edwards, K., Cesler-Maloney, M., Burns, A. J., Dibb, J., Simpson, W., Shiraiwa, M., Alexander, B., Mao, J., Flynn III, J. H., Stutz, J., and Anastasio, C.: Surprisingly robust photochemistry in subarctic particles during winter: evidence from photooxidants, *Atmospheric Chemistry and Physics*, 25, 9561–9581, <https://doi.org/10.5194/acp-25-9561-2025>, publisher: Copernicus GmbH, 2025.

Hems, R. F., Schnitzler, E. G., Liu-Kang, C., Cappa, C. D., and Abbatt, J. P.: Aging of Atmospheric Brown Carbon Aerosol, *ACS Earth and Space Chemistry*, 5, 722–748, <https://doi.org/10.1021/acsearthspacechem.0c00346>, publisher: American Chemical Society, 2021.

750 Kabanov, V., Ghosh, S., Lovell, J. F., and Heyne, B.: Singlet oxygen partition between the outer-, inner- and membrane-phases of photo/chemotherapeutic liposomes, *Physical Chemistry Chemical Physics*, 21, 25 054–25 064, <https://doi.org/10.1039/C9CP05159G>, publisher: The Royal Society of Chemistry, 2019.

Kaur, R. and Anastasio, C.: Light absorption and the photoformation of hydroxyl radical and singlet oxygen in fog waters, *Atmospheric Environment*, 164, 387–397, <https://doi.org/10.1016/j.atmosenv.2017.06.006>, 2017.

755 Kaur, R. and Anastasio, C.: First Measurements of Organic Triplet Excited States in Atmospheric Waters, *Environ. Sci. Technol.*, 52, 5218, 2018.

Kaur, R., Hudson, B. M., Draper, J., Tantillo, D. J., and Anastasio, C.: Aqueous reactions of organic triplet excited states with atmospheric alkenes, *Atmospheric Chemistry and Physics*, 19, 5021–5032, <https://doi.org/10.5194/acp-19-5021-2019>, 2019a.

760 Kaur, R., Labins, J. R., Helbock, S. S., Jiang, W., Bein, K. J., Zhang, Q., and Anastasio, C.: Photooxidants from Brown Carbon and Other Chromophores in Illuminated Particle Extracts, *Atmos. Chem. Phys.*, 19, 6579, 2019b.

Klein, G. W., Bhatia, K., Madhavan, V., and Schuler, R. H.: Reaction of hydroxyl radicals with benzoic acid. Isomer distribution in the radical intermediates, *The Journal of Physical Chemistry*, 79, 1767–1774, <https://doi.org/10.1021/j100584a005>, publisher: American Chemical Society, 1975.

765 Laskin, A., Laskin, J., and Nizkorodov, S. A.: Chemistry of Atmospheric Brown Carbon, *Chem. Rev.*, 115, 4335, 2015.



Laszakovits, J. R., Berg, S. M., Anderson, B. G., O'Brien, J. E., Wammer, K. H., and Sharpless, C. M.: p-Nitroanisole/pyridine and p-nitroacetophenone/pyridine actinometers revisited: Quantum yield in comparison to ferrioxalate, *Environmental Science & Technology Letters*, 4, 11–14, <https://doi.org/10.1021/acs.estlett.6b00422>, 2017.

Lee, H. J. J., Aiona, P. K., Laskin, A., Laskin, J., and Nizkorodov, S. A.: Effect of Solar Radiation on the Optical Properties and Molecular Composition of Laboratory Proxies of Atmospheric Brown Carbon, *Environmental Science & Technology*, 48, 10217–10226, <https://doi.org/10.1021/es502515r>, 2014.

Leresche, F., Salazar, J. R., Pfotenhauer, D. J., Hannigan, M. P., Majestic, B. J., and Rosario-Ortiz, F. L.: Photochemical Aging of Atmospheric Particulate Matter in the Aqueous Phase, *Environmental Science & Technology*, 55, 13152–13163, <https://doi.org/10.1021/acs.est.1c00978>, publisher: American Chemical Society, 2021.

775 Li, F., Lv, J., He, A., Xu, J., Zhao, L., Wang, X., Mao, L., Li, S., Wang, H., Wang, Y., and Jiang, G.: Unexpected Generation of Singlet Oxygen at the Air–Water Interface of Aqueous Microdroplets, *Journal of the American Chemical Society*, 147, 30574–30581, <https://doi.org/10.1021/jacs.5c02431>, publisher: American Chemical Society, 2025a.

Li, J., Chen, Q., and Guan, D.: Insights into the triplet photochemistry of atmospheric aerosol and subfractions isolated with different polarity, *Atmospheric Environment*, 290, 119375, <https://doi.org/10.1016/j.atmosenv.2022.119375>, 2022.

780 Li, Y., Fu, T.-M., Yu, J. Z., Zhang, A., Yu, X., Ye, J., Zhu, L., Shen, H., Wang, C., Yang, X., Tao, S., Chen, Q., Li, Y., Li, L., Che, H., and Heald, C. L.: Nitrogen dominates global atmospheric organic aerosol absorption, *Science*, 387, 989–995, <https://doi.org/10.1126/science.adr4473>, publisher: American Association for the Advancement of Science, 2025b.

Liu, Y., Li, Y., Chan, W. L., Bao, Y., Lee, P. K. H., and Nah, T.: Efficient Production of Reactive Oxidants by Atmospheric Bacterial-Derived Organic Matter in the Aqueous Phase, *Environmental Science & Technology*, 59, 6757–6770, <https://doi.org/10.1021/acs.est.5c01526>, publisher: American Chemical Society, 2025.

785 Lyu, Y., Lam, Y. H., Li, Y., Borduas-Dedekind, N., and Nah, T.: Seasonal variations in the production of singlet oxygen and organic triplet excited states in aqueous PM_{2.5} in Hong Kong SAR, South China, *Atmospheric Chemistry and Physics*, 23, 9245–9263, <https://doi.org/10.5194/acp-23-9245-2023>, publisher: Copernicus GmbH, 2023.

Ma, L., Guzman, C., Niedek, C., Tran, T., Zhang, Q., and Anastasio, C.: Kinetics and Mass Yields of Aqueous Secondary Organic 790 Aerosol from Highly Substituted Phenols Reacting with a Triplet Excited State, *Environmental Science & Technology*, 55, 5772–5781, <https://doi.org/10.1021/acs.est.1c00575>, publisher: American Chemical Society, 2021.

Ma, L., Worland, R., Jiang, W., Niedek, C., Guzman, C., Bein, K. J., Zhang, Q., and Anastasio, C.: Predicting photooxidant concentrations in aerosol liquid water based on laboratory extracts of ambient particles, *Atmospheric Chemistry and Physics*, 23, 8805–8821, <https://doi.org/10.5194/acp-23-8805-2023>, publisher: Copernicus GmbH, 2023a.

795 Ma, L., Worland, R., Tran, T., and Anastasio, C.: Evaluation of Probes to Measure Oxidizing Organic Triplet Excited States in Aerosol Liquid Water, *Environmental Science & Technology*, 57, 6052–6062, <https://doi.org/10.1021/acs.est.2c09672>, publisher: American Chemical Society, 2023b.

Ma, L., Worland, R., Heinlein, L., Guzman, C., Jiang, W., Niedek, C., Bein, K. J., Zhang, Q., and Anastasio, C.: Seasonal variations in photooxidant formation and light absorption in aqueous extracts of ambient particles, *Atmospheric Chemistry and Physics*, 24, 1–21, <https://doi.org/10.5194/acp-24-1-2024>, publisher: Copernicus GmbH, 2024.

800 Mabato, B. R. G., Lyu, Y., Ji, Y., Li, Y. J., Huang, D. D., Li, X., Nah, T., Lam, C. H., and Chan, C. K.: Aqueous secondary organic aerosol formation from the direct photosensitized oxidation of vanillin in the absence and presence of ammonium nitrate, *Atmospheric Chemistry and Physics*, 22, 273–293, <https://doi.org/10.5194/acp-22-273-2022>, publisher: Copernicus GmbH, 2022.



805 Maizel, A. C., Li, J., and Remucal, C. K.: Relationships Between Dissolved Organic Matter Composition and Photochemistry in Lakes of Diverse Trophic Status, *Environmental Science & Technology*, 51, 9624–9632, <https://doi.org/10.1021/acs.est.7b01270>, publisher: American Chemical Society, 2017.

810 Manfrin, A., Nizkorodov, S. A., Malecha, K. T., Getzinger, G. J., McNeill, K., and Borduas-Dedekind, N.: Reactive Oxygen Species Production from Secondary Organic Aerosols: The Importance of Singlet Oxygen, *Environmental Science & Technology*, 53, 8553–8562, <https://doi.org/10.1021/acs.est.9b01609>, 2019.

815 Marchisio, A., Minella, M., Maurino, V., Minero, C., and Vione, D.: Photogeneration of reactive transient species upon irradiation of natural water samples: Formation quantum yields in different spectral intervals, and implications for the photochemistry of surface waters, *Water Research*, 73, 145–156, <https://doi.org/10.1016/j.watres.2015.01.016>, 2015.

820 McNeill, K. and Canonica, S.: Triplet state dissolved organic matter in aquatic photochemistry: reaction mechanisms, substrate scope, and photophysical properties, *Environmental Science: Processes & Impacts*, 18, 1381–1399, <https://doi.org/10.1039/C6EM00408C>, publisher: The Royal Society of Chemistry, 2016.

825 Mir, M., Jansen, L. M. G., Wilkinson, F., Bourdelande, J. L., and Marquet, J.: Efficiency of singlet oxygen generation from the triplet states of nitrophenyl ethers, *Journal of Photochemistry and Photobiology A: Chemistry*, 113, 113–117, [https://doi.org/10.1016/S1010-6030\(97\)00325-0](https://doi.org/10.1016/S1010-6030(97)00325-0), 1998.

830 Myers-Pigg, A. N., Griffin, R. J., Louchouarn, P., Norwood, M. J., Sterne, A., and Cevik, B. K.: Signatures of Biomass Burning Aerosols in the Plume of a Saltmarsh Wildfire in South Texas, *Environmental Science & Technology*, 50, 9308–9314, <https://doi.org/10.1021/acs.est.6b02132>, 2016.

NIST, N. O. o. D. a.: Oxygen, <https://webbook.nist.gov/cgi/cbook.cgi?ID=C7782447&Mask=10>, publisher: National Institute of Standards and Technology.

825 Nonell, S. and Flors, C.: Steady-State and Time-Resolved Singlet Oxygen Phosphorescence Detection in the Near-IR, <https://doi.org/10.1039/9781782626992-00007>, 2016.

Ossola, R., Jönsson, O. M., Moor, K., and McNeill, K.: Singlet Oxygen Quantum Yields in Environmental Waters, *Chemical Reviews*, 121, 4100–4146, <https://doi.org/10.1021/acs.chemrev.0c00781>, 2021.

830 Partanen, S. B., Erickson, P. R., Latch, D. E., Moor, K. J., and McNeill, K.: Dissolved Organic Matter Singlet Oxygen Quantum Yields: Evaluation Using Time-Resolved Singlet Oxygen Phosphorescence, *Environmental Science & Technology*, 54, 3316–3324, <https://doi.org/10.1021/acs.est.9b07246>, publisher: American Chemical Society, 2020.

Partanen, S. B., Apell, J. N., Lin, J., and McNeill, K.: Factors affecting the mixed-layer concentrations of singlet oxygen in sunlit lakes, *Environmental Science: Processes & Impacts*, 23, 1130–1145, <https://doi.org/10.1039/D1EM00062D>, publisher: The Royal Society of Chemistry, 2021.

835 Petersen-Sonn, E. A., Brigante, M., Deguillaume, L., Jaffrezo, J.-L., Perrier, S., and George, C.: Evaluating the potential secondary contribution of photosensitized chemistry to OH production in aqueous aerosols, *Environmental Science: Atmospheres*, 4, 1170–1182, <https://doi.org/10.1039/D4EA00103F>, publisher: RSC, 2024.

Petersen-Sonn, E. A., Brigante, M., Deguillaume, L., Jaffrezo, J.-L., and George, C.: Tropospheric Multiphase Chemistry: Excited Triplet States Compete with OH Radicals and Singlet Molecular Oxygen, *ACS Earth and Space Chemistry*, 9, 533–544, <https://doi.org/10.1021/acsearthspacechem.4c00295>, publisher: American Chemical Society, 2025.



840 Redmond, R. W. and Gamlin, J. N.: A Compilation of Singlet Oxygen Yields from Biologically Relevant
Molecules, *Photochemistry and Photobiology*, 70, 391–475, <https://doi.org/10.1111/j.1751-1097.1999.tb08240.x>, _eprint:
<https://onlinelibrary.wiley.com/doi/pdf/10.1111/j.1751-1097.1999.tb08240.x>, 1999.

845 Samburova, V., Connolly, J., Gyawali, M., Yatavelli, R. L. N., Watts, A. C., Chakrabarty, R. K., Zielinska, B., Moosmüller, H., and Khlystov,
A.: Polycyclic aromatic hydrocarbons in biomass-burning emissions and their contribution to light absorption and aerosol toxicity, *Science
of The Total Environment*, 568, 391–401, <https://doi.org/10.1016/j.scitotenv.2016.06.026>, 2016.

Schmidt, R., Tanielian, C., Dunsbach, R., and Wolff, C.: Phenalenone, a universal reference compound for the determination of
quantum yields of singlet oxygen $O_2(1\Delta g)$ sensitization, *Journal of Photochemistry and Photobiology A: Chemistry*, 79, 11–17,
[https://doi.org/10.1016/1010-6030\(93\)03746-4](https://doi.org/10.1016/1010-6030(93)03746-4), 1994.

850 Schweitzer, C. and Schmidt, R.: Physical Mechanisms of Generation and Deactivation of Singlet Oxygen, *Chemical Reviews*, 103, 1685–
1758, <https://doi.org/10.1021/cr010371d>, publisher: American Chemical Society, 2003.

Schweitzer, C., Mehrdad, Z., Noll, A., Grabner, E.-W., and Schmidt, R.: Mechanism of Photosensitized Generation of Singlet Oxygen during
Oxygen Quenching of Triplet States and the General Dependence of the Rate Constants and Efficiencies of $O_2(1\Sigma g^+)$, $O_2(1\Delta g)$, and
 $O_2(3\Sigma g^-)$ Formation on Sensitizer Triplet State Energy and Oxidation Potential, *The Journal of Physical Chemistry A*, 107, 2192–2198,
<https://doi.org/10.1021/jp026189d>, publisher: American Chemical Society, 2003.

855 Shakya, K. M., Loucheurn, P., and Griffin, R. J.: Lignin-Derived Phenols in Houston Aerosols: Implications for Natural Background
Sources, *Environmental Science & Technology*, 45, 8268–8275, <https://doi.org/10.1021/es201668y>, 2011.

Sharpless, C. M.: Lifetimes of Triplet Dissolved Natural Organic Matter (DOM) and the Effect of $NaBH_4$ Reduction on Singlet
Oxygen Quantum Yields: Implications for DOM Photophysics, *Environmental Science & Technology*, 46, 4466–4473,
<https://doi.org/10.1021/es300217h>, publisher: American Chemical Society, 2012.

860 Siemens, K. S. A., Pagonis, D., Guo, H., Schueneman, M. K., Dibb, J. E., Campuzano-Jost, P., Jimenez, J. L., and Laskin, A.: Probing
Atmospheric Aerosols by Multimodal Mass Spectrometry Techniques: Revealing Aging Characteristics of Its Individual Molecular Com-
ponents, *ACS Earth and Space Chemistry*, <https://doi.org/10.1021/acsearthspacechem.3c00228>, publisher: American Chemical Society,
2023.

865 Smith, J. D., Sio, V., Yu, L., Zhang, Q., and Anastasio, C.: Secondary Organic Aerosol Production from Aqueous Reactions of Atmospheric
Phenols with an Organic Triplet Excited State, *Environmental Science & Technology*, 48, 1049–1057, <https://doi.org/10.1021/es4045715>,
publisher: American Chemical Society, 2014.

Smith, J. D., Kinney, H., and Anastasio, C.: Phenolic carbonyls undergo rapid aqueous photodegradation to form low-volatility, light-
absorbing products, *Atmospheric Environment*, 126, 36–44, <https://doi.org/10.1016/j.atmosenv.2015.11.035>, 2016.

870 Tymstra, C., Stocks, B. J., Cai, X., and Flannigan, M. D.: Wildfire management in Canada: Review, challenges and opportunities, *Progress
in Disaster Science*, 5, 100 045, <https://doi.org/10.1016/j.pdisas.2019.100045>, 2020.

Valiev, R. R., He, Y., Weltzin, T., Zhu, A., Lee, D., Moore, E., Gee, A., Drozd, G., and Kurten, T.: Wavelength-dependent in-
tersystem crossing dynamics of phenolic carbonyls in wildfire emissions, *Physical Chemistry Chemical Physics*, 27, 998–1007,
<https://doi.org/10.1039/D4CP03501A>, publisher: The Royal Society of Chemistry, 2025.

875 Wilkinson, F., Helman, W. P., and Ross, A. B.: Quantum Yields for the Photosensitized Formation of the Lowest Electroni-
cally Excited Singlet State of Molecular Oxygen in Solution, *Journal of Physical and Chemical Reference Data*, 22, 113–262,
<https://doi.org/10.1063/1.555934>, 1993.



Wu, B., Liu, T., Wang, Y., Zhao, G., Chen, B., and Chu, C.: High Sample Throughput LED Reactor for Facile Characterization of the Quantum Yield Spectrum of Photochemically Produced Reactive Intermediates, *Environmental Science & Technology*, <https://doi.org/10.1021/acs.est.1c04608>, publisher: American Chemical Society, 2021.

880 Xu, J., Cui, T., Fowler, B., Fankhauser, A., Yang, K., Surratt, J. D., and McNeill, V. F.: Aerosol Brown Carbon from Dark Reactions of Syringol in Aqueous Aerosol Mimics, *ACS Earth Space Chem.*, 2, 608, 2018.

Xu, J., Hettiyadura, A. P. S., Liu, Y., Zhang, X., Kang, S., and Laskin, A.: Atmospheric Brown Carbon on the Tibetan Plateau: Regional Differences in Chemical Composition and Light Absorption Properties, *Environmental Science & Technology Letters*, 9, 219–225, <https://doi.org/10.1021/acs.estlett.2c00016>, publisher: American Chemical Society, 2022.

885 Zhang, J., Shrivastava, M., Ma, L., Jiang, W., Anastasio, C., Zhang, Q., and Zelenyuk, A.: Modeling Novel Aqueous Particle and Cloud Chemistry Processes of Biomass Burning Phenols and Their Potential to Form Secondary Organic Aerosols, *Environmental Science & Technology*, 58, 3776–3786, <https://doi.org/10.1021/acs.est.3c07762>, publisher: American Chemical Society, 2024.

900 Zheng, P., Chen, Y., Wang, Z., Liu, Y., Pu, W., Yu, C., Xia, M., Xu, Y., Guo, J., Guo, Y., Tian, L., Qiao, X., Huang, D. D., Yan, C., Nie, W., Worsnop, D. R., Lee, S., and Wang, T.: Molecular Characterization of Oxygenated Organic Molecules and Their Dominating Roles in Particle Growth in Hong Kong, *Environmental Science & Technology*, 57, 7764–7776, <https://doi.org/10.1021/acs.est.2c09252>, publisher: American Chemical Society, 2023.

895 Zhou, X., Davis, A. J., Kieber, D. J., Keene, W. C., Maben, J. R., Maring, H., Dahl, E. E., Izaguirre, M. A., Sander, R., and Smoydzyn, L.: Photochemical production of hydroxyl radical and hydroperoxides in water extracts of nascent marine aerosols produced by bursting bubbles from Sargasso seawater, *Geophysical Research Letters*, 35, [https://doi.org/https://doi.org/10.1029/2008GL035418](https://doi.org/10.1029/2008GL035418), _eprint: <https://agupubs.onlinelibrary.wiley.com/doi/pdf/10.1029/2008GL035418>, 2008.